Organisation of afferents along the anterior-posterior and medial-lateral axes of the rat OFC

Ines V. Barreiros[*,1, 2, 3], Marios C. Panayi[*,1, 3], Mark E. Walton[1,3]

* equal contribution

1. Department of Experimental Psychology, University of Oxford
2. Nuffield Department of Clinical Neurosciences, University of Oxford
3. Wellcome Centre for Integrative Neuroimaging, University of Oxford

Correspondence should be addressed to:

Ines V. Barreiros, ines.barreiros@chch.ox.ac.uk, Department of Experimental Psychology, University of Oxford, Tinsley Building, Mansfield Road, Oxford OX1 3SR, UK

Mark E. Walton, mark.walton@psy.ox.ac.uk, Department of Experimental Psychology, University of Oxford, Tinsley Building, Mansfield Road, Oxford OX1 3SR, UK

Abstract

The orbitofrontal cortex (OFC) has been anatomically divided into a number of subregions along its medial-lateral axis, which behavioural research suggests have distinct functions. Recently, evidence has emerged suggesting functional diversity is also present along the rostral-caudal axis of the rodent OFC. However, the patterns of anatomical connections that underlie these differences have not been well characterised. Here, we use the retrograde tracer cholera toxin subunit B to simultaneously label the projections into the anterior lateral (ALO) and posterior lateral (PLO), and posterior ventral (PVO) portions of the rat OFC. Our methodological approach allowed to us to simultaneously compare the density and input patterns into these OFC subdivisions. We observed distinct and topographically organised projection patterns into ALO, PLO and PVO from the mediodorsal and the submedius nuclei of the thalamus. We also observed different levels of connectivity strength into these OFC subdivisions from the amygdala, motor cortex, sensory cortices and medial prefrontal cortical structures, including medial OFC, infralimbic and prelimbic cortices. Interestingly, while labelling in some of these input regions revealed only a gradient in connectivity strength, other regions seem to project almost exclusively to specific OFC subdivisions. Moreover, differences in input patterns between ALO and PLO were as pronounced as those between PLO and PVO. Together, our results support the existence of distinct anatomical circuits within lateral OFC along its anterior-posterior axis.

***Keywords*:** anterior-posterior; medial-lateral; neuroanatomy; orbitofrontal cortex; submedius thalamus.

Abbreviations

AI, d, v	agranular insular cortex, dorsal, ventral divisions
ACC	anterior cingulate cortex
ALO	lateral orbitofrontal cortex, anterior part
AVO	ventral orbitofrontal cortex, anterior part
BLA	basolateral nucleus of amygdala
BLP	basolateral nucleus of the amygdala, posterior part
DLO	dorsolateral orbitofrontal cortex
DP	dorsal peduncular cortex
FrA	frontal association cortex
GI	gustatory insular cortex
IL	infralimbic cortex
LaDL	lateral amygdala, dorsolateral part
LaVL	lateral amygdala, ventrolateral part
LaVM	lateral amygdala, ventromedial part
LO	lateral orbitofrontal cortex
M1	primary motor cortex
M2	secondary motor cortex
MD, m, c, l	mediodorsal nucleus of the thalamus, medial, central, lateral parts
MO	medial orbitofrontal cortex
NAc	nucleus accumbens
NAc, C, S	nucleus accumbens, core, shell
PL	prelimbic cortex
PLO	lateral orbitofrontal cortex, posterior part
PT	paratenial nucleus of the thalamus
PVO	ventral orbitofrontal cortex, ventral part
Re	nucleus reuniens of the thalamus
S1J	primary somatosensory cortex, jaw region
Sub, D, V	submedius nucleus of the thalamus, dorsal, ventral parts
VO	ventral orbitofrontal cortex

Introduction

Over recent years there has been an increasing understanding that the rodent orbitofrontal cortex (OFC) is not functional homogenous, particularly along its medial-lateral axis (see Barreiros, Ishii, Walton, & Panayi, 2020; Bradfield & Hart, 2020; Izquierdo, 2017 for reviews). A recent review (Izquierdo, 2017) looked at the relationship between the functions reported in rat OFC studies and the anatomical placement of the recording or manipulation sites. This revealed that functional heterogeneity can be mapped, to a certain degree, onto the divisions established by classical OFC parcellation methods. These classical parcellation studies define OFC subregions predominantly along the medial-lateral axis, including medial (MO), ventral (VO), ventrolateral (VLO), lateral (LO), dorsolateral (DLO) and agranular insular (AI) portions (Krettek & Price, 1977b; Price, 2006; Ray & Price, 1992).

While cytoarchitectural, neuroanatomical and behavioural studies have mostly focused on the medial-lateral axis, recent reports suggest that there may also be important distinctions along the anterior-posterior axis. For example, Panayi & Killcross (2018) found that, while either anterior or posterior LO lesions impaired Pavlovian outcome devaluation, only posterior, but not anterior, LO lesions disrupted Pavlovian reversal learning. Another study revealed that the anterior but not posterior portion of MO is critical for inferring unobservable action-dependent outcomes and for behavioural response adaptation in outcome-devaluation tasks (Bradfield, Hart, & Balleine, 2018). These findings suggest that, rather than functionally uniform, the currently recognised OFC subregions (see Krettek & Price, 1977; Price, 2006; Ray & Price, 1992) might be composed of smaller structural and functional regions along its anterior-posterior axis. However, given the relative lack of clear cytoarchitectonic differences (Van De Werd & Uylings, 2008), it remains an open question whether there are anatomical distinctions that might underpin these functional differences.

Classically, the boundaries between prefrontal cortical regions, including OFC, have been defined by their specific projections patterns with the mediodorsal (MD) thalamus (Rose & Woolsey, 1948). Surprisingly, in comparison to other prefrontal cortical regions, there have been relatively few studies on the anatomical connectivity of the rat OFC, particularly looking at anterior versus posterior differences. Moreover, because there have been few studies systematically characterising the connectivity of different OFC subregions within the same subjects, inferences between subjects have often been necessary to make these comparisons.

Here, we test whether functional heterogeneity across the anterior-posterior axis of the OFC is underpinned by differences in anatomical connectivity, and with a focus on LO. Specifically, we test the hypothesis that there are distinct anatomical projections to the anterior lateral (ALO) and posterior lateral OFC (PLO) that underlie the functional dissociation reported by Panayi & Killcross (2018). We contrast these regions with the posterior ventral OFC (PVO) an anatomically adjacent portion of the OFC which is thought to be functionally distinct from LO (Balleine, Leung, & Ostlund, 2011; Corwin, Fussinger, Meyer, King, & Reep, 1994). Specifically, we use the retrograde tracer cholera toxin subunit B (CTB) to simultaneously characterise the afferent projections to these regions. This approach allows us to establish whether any differences reflect (1) a gradient of afferent projections that may be organised topographically, or (2) a unique pattern of inputs that projects exclusively to a single subregion.

Methods

Subjects

A total of 14 male Lister Hooded rats (Charles River), ~275-300 g in weight at the start of experiment (8-12 weeks old), were used in this study. Of these, 7 animals provided usable data (inclusion and exclusion criteria described below), 4 of which were triple-labelled and 3 single-labelled. Animals were housed in groups of 3 in polycarbonate cages, with ad libitum access

to water and food. The housing room was maintained at a room temperature of 23 ± 1ºC, humidity of 40 ± 10% and on 12-hour light/dark cycles beginning at 7 A.M., with lights during the day. All animal experimental procedures were approved and carried out in accordance with the British Home Office regulations and under the Animals (Scientific Procedures) Act 1986 (UK).

Surgery

Animals were placed in vaporization chambers and anesthetised initially with 4% isoflurane (2 L/min O_2) and maintained on 1–2% isoflurane (2 L/min O_2) for the rest of the procedure. After induction, the head was shaved, and the rat was secured in a stereotaxic frame (Kopf Instruments). Body temperature was maintained at 37 ± 0.5°C with the use of a homoeothermic heating blanket. Corneal dehydration was prevented with application of ophthalmic ointment (Lacri-Lube, Allergan). The scalp was cleaned with diluted hibiscrub and 70% ethanol, and a local anaesthetic, bupivacaine (2 mg/kg), was applied to the area. The skin on top of the head was retracted and holes were then drilled in the skull for the injections. 50 nl of retrograde tracer CTB coupled to Alexa-Fluor 488, 555 or 648 conjugate (C34775, C34776, C34778, Life Technologies) was microinjected through micropipettes with ~10-µm Ø pulled from thin-walled borosilicate glass capillaries (outer Ø: 1.14 mm, inner Ø: 0.53 mm; 3-000-203-G/X, Drummond Scientific) using a vertical micropipette puller (PE-2, Narishige) via an automated injector (Nanoject III, Drummond Scientific). Tracers were injected unilaterally, into the right hemisphere, at a rate of 1 nl/s. Each animal received injection of one of the 3 tracers into ALO, PLO, and PVO. Tracer-site combinations were counterbalanced across animals. Coordinates used were as indicated in Table 1. Before injection, the micropipette was lowered 0.2 mm below the intended injection sites and left in place for 1 min, before being raised to the injection site dorsoventral coordinate. Micropipettes were left in place for 5 min after each bolus

injection to ensure diffusion of tracer. Micropipettes were then slowly retracted, and the incision closed with vicryl sutures.

All animals were administered buprenorphine (0.1 ml/kg, s. c.), both pre- and post-surgically, and meloxicam (Metacam, 0.2/ml/kg, s. c.), post-surgically. Animals were then allowed to recover in thermostatically controlled cages and given palatable food for consumption. Meloxicam was also administered for at least 3 days following surgery.

Table 1

Coordinates used for tracer injection into OFC subdivisions

OFC subdivision	AP from bregma (mm)	ML from bregma (mm)	DV from dura (mm)
ALO	+3.70 (+4.20)	+2.50 (+2.60)	-3.30 (-3.50)
PLO	+2.70 (+3.20)	+3.30 (+3.40)	-4.40 (-4.70)
PVO	+2.70 (+3.20)	+1.90 (+2.00)	-4.40 (-4.50)

Note. Coordinates were experimentally adjusted based on a data from a pilot study to target the brain areas at the coordinates depicted in brackets in a standard rat brain atlas (Paxinos & Watson, 1998). AP: anteroposterior, ML: mediolateral, DV: dorsoventral. Based on the previously established functional boundary in LO (Panayi & Killcross, 2018), we used the presence of the corpus collosum and the claustrum in the coronal section to mark the anterior-posterior division.

Histology

Ten days after tracer injection, animals were administered a terminal dose of pentobarbitone (30-60 mg/kg). After loss of pedal reflex, the animals were perfused transcardially with 150 ml of phosphate buffer saline followed by 400 ml of 4% paraformaldehyde. The brains were removed, kept in paraformaldehyde for 24 h and then transferred to phosphate buffer saline. Before slicing, brains were cryoprotected in 30% sucrose solution. 60-µm thick coronal sections were obtained with a freezing microtome (Leitz). Sections were mounted onto slides and coverslipped with mounting medium with DAPI (H-1500 Vectashield, Vector Labs).

Image acquisition and analysis

Images were captured using a confocal slide scanner (Axio Scan.Z1, Zeiss) equipped with an air 20x/NA 0.8 objective. Levels of cell labelling density were manually categorised, offline, into four levels: 0, absence of labelling; 1, weak; 2, moderate; 3, strong. Areas with saturated labelling, only found around injection sites, were not included in the analyses. The classification of brain areas was based on a standard rat brain atlas (Paxinos & Watson, 1998). In our analysis, we focused on the quantification of frontal lobe structures, including OFC subdivisions, prelimbic, infralimbic, anterior cingulate cortex and motor cortex; temporal lobe structures, including amygdala, lateral entorhinal cortex and perirhinal cortex; retrosplenial cortex; primary sensory cortices; thalamic nuclei, including paratenial, submedius and mediodorsal. Due to difficulties in obtaining brain slices of consistent quality posterior to -5.30 mm from Bregma, we did not quantify labelling in midbrain structures.

In the description and interpretation of our results, we consider anterior and posterior portions of the medial, lateral and ventral OFC separately. We refer to the portions of LO and VO contained in the coronal slices from +4.70 to + 4.20 mm from Bregma as anterior and to those contained in the coronal slices from +3.20 to +2.20 mm as posterior, with the corpus collosum and the claustrum in the coronal section marking the anterior-posterior division as previously established for LO (Panayi & Killcross, 2018). Based on a previously observed functional dissociation in MO (Bradfield et al., 2018), we refer to the areas contained in coronal slices at +4.70 and +3.70 mm from Bregma as anterior and posterior MO, respectively. These coordinates are based on a standard rat brain atlas (Paxinos & Watson, 1998). While an area VLO has been proposed to exist between VO and LO, here we will only differentiate between areas VO and LO as per the boundaries defined in Paxinos & Watson (1998).

Experimental units (*n*) reported here are individual injection sites. Depiction of labelling in key areas of interest, including the amygdala, mediodorsal thalamus and submedius nucleus of the thalamus, was obtained by superimposing hand drawings of the labelling in each brain

using an opacity value proportional to the density level of labelling observed. The summary table and figure depicting the average labelling for each injection site are based on the density average across brains, subsequently averaged across slices when a single slice is represented and discretised into four density values: –, absence of labelling; +, weak; ++ moderate; +++ – strong (Table 2 and Figure 1). The weak density level (+) also includes any region that is consistently labelled, i.e. across at least 50% of the brains, even if only very sparse labelling was observed. Data from injections that were off target (n = 11), in which tracer did not diffuse (n = 8), were both off target and the tracer did not diffuse (n = 6), or in which the tracer diffused into the white matter (n = 2) were excluded from all analyses (see Figure S1).

Results

Simultaneous characterisation of ALO, PLO and PVO afferents

We set out to simultaneously characterise the inputs of three distinct portions of the rat OFC: ALO, PLO, and PVO. We compared the projections of the three subdivisions in the same brain, while using the same retrograde tracer (cholera toxin subunit B, CTB), coupled to different fluorescent dyes (Conte, Kamishina, & Reep, 2009). The data presented here was obtained from 7 brains: 4 triple-, 3 single-labelled. Figure 1 illustrates the intended injection sites and the core of tracer deposits observed following histological analysis of injected brains. The location of the core injection deposits included in the analysis were mostly confined to the intended OFC subdivision, with some extension into the ventral agranular insula (AIv) from the PLO injections. The localisation and average density of retrogradely-labelled cells observed are illustrated in Figure 2 (see Table S1 in the supplemental material for exact average density values). Labelling in each individual brain following tracer deposition into ALO, PLO and

PVO is represented in Supplementary Figures S2, S3, and S4, respectively, in the supplemental material.

In our study, contralateral labelling was limited to prefrontal afferents (ending at +2.20 mm from bregma; Figure 2). The remaining labelling was observed only ipsilaterally. In the triple-labelled brains the vast majority of cells were single-labelled with only a small proportion of cells being double- or triple-labelled. These were particularly prevalent in the submedius nucleus of the thalamus. The density of the retrogradely-labelled cells observed in key areas of interest is summarised in Table 2.

Prefrontal cortex afferents

Intra-OFC projections

Dorsolateral OFC: following injection of CTB into ALO, we observed strong labelling in the dorsolateral portion of the OFC (DLO), ipsi- and contralaterally to the injection site, with ipsilateral labelling being stronger (Figure 2). In contrast, we detected weak or no labelling in this OFC portion following injection into PLO or PVO, respectively, both ipsi- and contralaterally.

Agranular insula: following ALO injection, we detected only a few labelled cells in the agranular insula (AI) of the same coronal plane as the injection site and weak to moderate labelling in posterior slices. PLO injection resulted in weak or very strong ipsilateral labelling in anterior and posterior AI, respectively. Retrograde labelling in the contralateral side was mostly weaker. PVO injection resulted in weak to moderate density of labelled cells in the posterior portions of AI.

Lateral OFC: ALO injections of CTB resulted in very strong labelling and strong labelling in ALO and PLO, respectively, ipsilaterally to the injection site. This was largely mirrored on the contralateral hemisphere. PLO injections resulted in very strong labelling in PLO and only

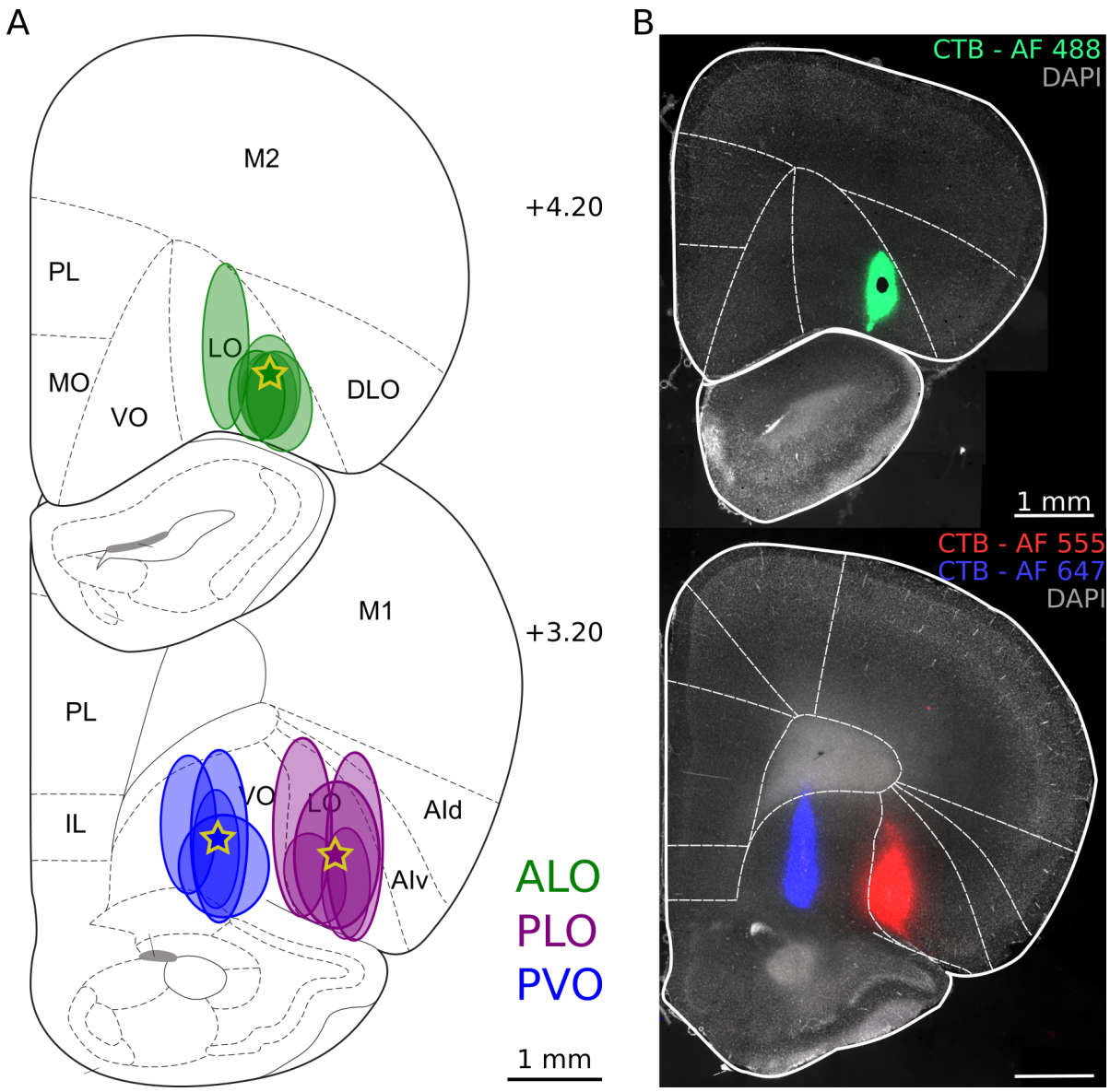

Figure 1. **Coronal sections depicting core of tracer deposits into ALO, PLO and PVO, illustrated at the level of maximal deposit.** (A) Stars and oval shapes represent the intended and the observed injection sites core, respectively. Injections whose core fell outside the orbitofrontal cortex or in which the tracer did not diffuse are not represented here (see instead Figure S1). *n* ALO = 6, *n* PLO = 5, *n* PVO = 4 injections. (B) Example injection sites of triple-labelled brain. Distances shown are distances from bregma in mm. ACC1: anterior cingulate cortex, area 1; AI: agranular insular cortex; AId: agranular insular cortex, dorsal part; AIv: agranular insular cortex, ventral part; DLO: orbitofrontal cortex, dorsolateral area; DP: dorsal peduncular cortex; IL: infralimbic cortex; GI: gustatory insular cortex; MO: orbitofrontal cortex, medial area; LO: orbitofrontal cortex, lateral area; Pir: piriform cortex; PL: prelimbic cortex; M1: primary motor cortex; M2: secondary motor cortex; NAcC: nucleus accumbens, core; NAcS: nucleus accumbens, shell; S1J: primary somatosensory cortex, jaw region; VO: orbitofrontal cortex, ventral area; CTB: cholera toxin subunit B; AF – Alexa Fluor.

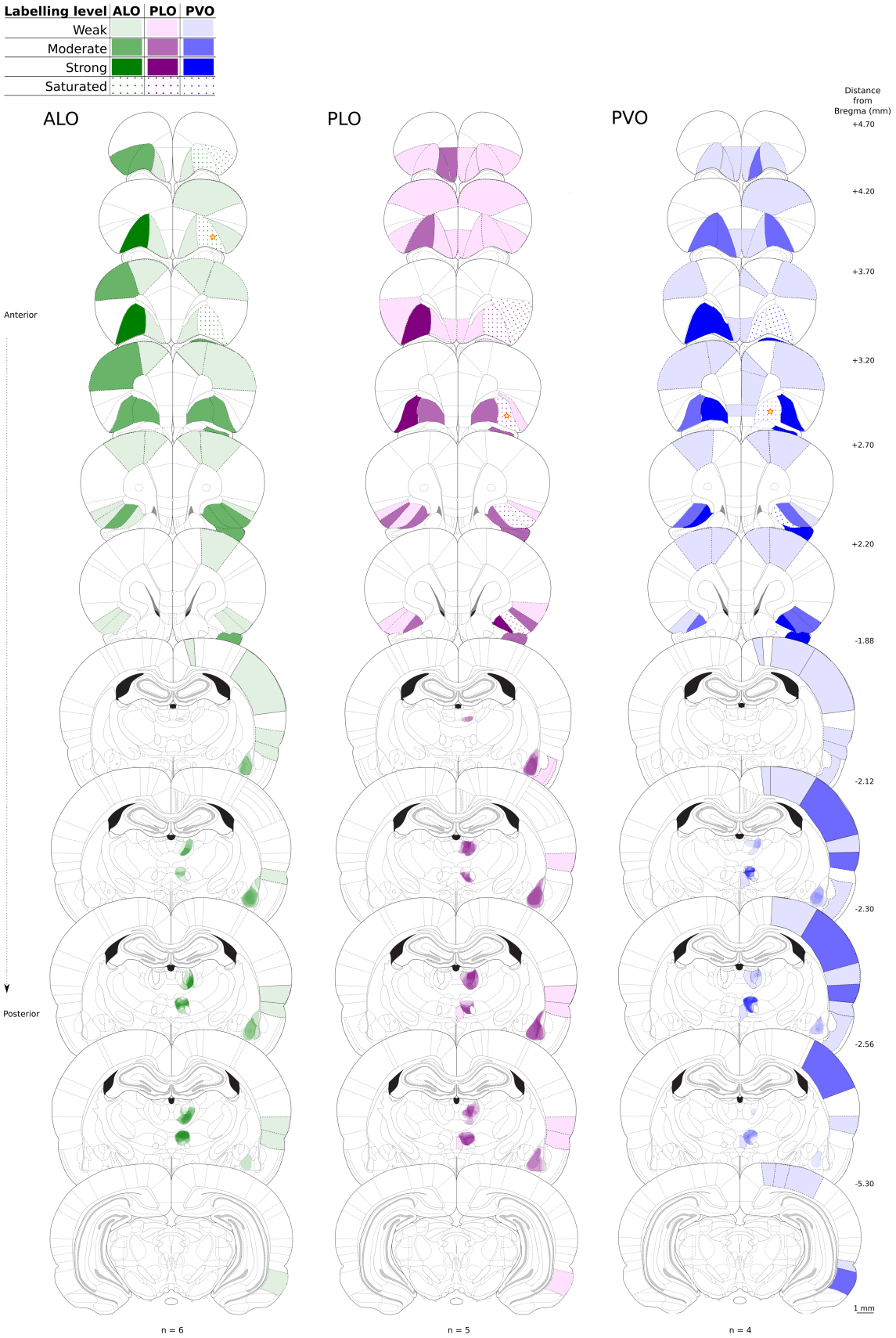
Labelling level
ALO
PLO
PVO
Weak
Moderate
Strong
Saturated
ALO
PLO
PVO
Distance from Bregma (mm)
+4.70
+4.20
+3.70
+3.20
+2.70
+2.20
-1.88
-2.12
-2.30
-2.56
-5.30
Anterior
Posterior
1 mm
n = 6
n = 5
n = 4

Figure 2. **Density of retrogradely-labelled cells following CTB injection into ALO, PLO or PVO.** Represented is the average density across brains discretised into four labelling levels (see Table S1 for exact average density values). Lighter or darker shades represent lower or higher labelling densities, respectively. Depiction of labelling in key areas of interest (amygdala, mediodorsal thalamus and submedius nucleus of the thalamus) was obtained by superimposing hand drawings of the labelling in each brain using an opacity value proportional to the density level of labelling observed. Star shapes represent the intended injection site cores. *n* ALO = 6, *n* PLO = 5, *n* PVO = 4.

weak labelling in ALO, ipsilaterally. Contralaterally, we detected weak to moderate labelling in ALO and weak to dense labelling in PLO. Following injection of CTB into PVO, we observed moderate to very strong labelling in PLO and only weak to moderate labelling in ALO, ipsilaterally. This was largely mirrored on the contralateral hemisphere.

Ventral OFC: Following tracer injection into ALO, we detected only a few labelled cells in anterior ventral OFC (AVO) but moderate labelling in PVO, ipsilaterally. A similar labelling pattern was observed following tracer injection into PLO. This was largely mirrored on the contralateral hemisphere both in ALO and PLO injections. Injection into PVO resulted in weak or very strong labelling in ipsilateral AVO or PVO, respectively. Retrograde labelling in the contralateral side largely mirrored that of the ipsilateral cortex, generally with fewer cells present.

Medial OFC: The medial portion of the OFC (MO) had almost no labelled cells following ALO injection, with only some very low-density labelling in its most anterior part in both hemispheres in 2 of the 6 brains included in the analysis (see Figure S2). By contrast, both PLO and PVO injections resulted in weak labelling in both the anterior and posterior portions of MO, ipsilaterally. A similar pattern was observed in the contralateral hemisphere, with the exception that the anterior portion of MO contained stronger labelling contralateral to the injection site following PVO injection.

In summary, all three subdivisions receive input from most other parts of the OFC, both ipsi- and contralaterally. One distinction is MO, which sends stronger projections to PLO and PVO than to ALO.

Medial prefrontal projections

Following retrograde tracer injection into ALO, prelimbic (PL) and infralimbic (PL) were mostly devoid of labelled cells, both ipsi- and contralaterally (Figure S2). On the other hand, following PLO injection, both IL and PL contained weak labelling in 3 of the 5 brains included in the analysis either ipsi- or contralaterally to the injection site. Similarly, we observed weak labelling in both IL and PL following PVO injection.

No labelled cells were detected consistently in the anterior cingulate cortex (ACC), in either hemisphere following injection into ALO or PLO. By contrast, PVO injection often resulted in light labelling in this region (Figure 2, Figure S4).

Thus, IL and PL labelling suggest an anterior-posterior difference within LO, while ACC labelling suggests a medial-lateral distinction between PLO and PVO.

Motor cortex

Following injections into ALO and PVO, we observed sparse labelled cells in both ipsilateral, primary (M1) and secondary motor (M2) cortices (Figure 2). This was largely mirrored in the contralateral side with the difference that, here, ALO resulted in moderate labelling in M1. By contrast, PLO injection resulted only in weak labelling restricted to M2, both ipsi- and contralaterally. Overall, input from motor cortices suggest both an anterior-posterior difference, and a medial-lateral difference such that PLO receives much weaker motor inputs than ALO and PVO.

Sensory cortices

In sensory cortices, we observed labelling only ipsilaterally to the tracer injections (Figure 2). Following CTB injection into PVO, but not ALO or PLO, we observed weak labelling present in the lateral, mediolateral and mediomedial areas of the secondary visual cortex, and weak to moderate labelling in the barrel cortex and in the forelimb, hindlimb and trunk regions of the primary somatosensory cortex, ipsilaterally. In contrast, except for weak labelling in the barrel cortex after ALO injection, we observed no labelled cells in the visual or the somatosensory cortices following injection into lateral OFC (either ALO or PLO). Following injection into either ALO, PLO or PVO, we detected moderate and weak labelling in piriform and gustatory insular cortices, respectively. However, posterior to -1.88 mm from Bregma, the piriform cortex exhibited only weak labelling from PVO injections. The auditory cortex was devoid of labelled cells following injection into either subdivision. Therefore, there was strong evidence of primary multi-sensory inputs into PVO, but not into ALO or PLO.

Temporal lobe

In the temporal lobe, we detected labelled cells only in the hemisphere ipsilateral to the injection site (Figure 2). Lateral entorhinal cortex exhibited weak labelling following injection into either ALO or PLO but stronger labelling following PVO injection. Labelling was also detected in the perirhinal cortex after tracer injection into PVO but was not consistently present following ALO or PLO injections (see Figure S1 and S2). Hippocampal formation structures did not contain labelled cells following injection into either ALO, PLO or PVO. In summary, although labelling in the entorhinal and perirhinal was not always consistent, the labelling patterns observed suggest a gradient between their inputs into LO and VO.

Amygdala

A detailed schematic for the amygdala is shown in Figures 3 and 4, including hand drawn overlays for each brain at each injection site (Figure 3-A) and histological images from a representative triple labelled brain (Figure 3-B). In the amygdala, we observed labelling only ipsilaterally to the tracer injection. The anterior part of the basolateral amygdala (BLA) exhibited moderate labelling following PLO injection but only weak labelling after either ALO or PVO injections (Figure 3-A right). We observed a similar pattern in the dorsolateral part of the lateral amygdala (LaDL), with the difference that it did not contain labelled cells following PVO injection. We detected weak labelling in the posterior part of the basolateral amygdala (BLP) and in the ventromedial (LaVM) and ventrolateral (LaVL) parts of the lateral amygdala only following tracer injection into PLO. There was no labelling in other parts of the amygdala. Overall, amygdala labelled cells were most prevalent in BLA and following injection into PLO, suggesting both an anterior-posterior gradient within LO and a medial-lateral gradient between PLO and PVO. There were no labelled cells outside of the basolateral and lateral regions of the amygdala.

Thalamus

In the thalamus, we observed labelled cells only ipsilaterally to the injection site of the retrograde tracer (Figure 2). As with the amygdala, detailed schematics for this region are shown in Figures 5-7, including hand drawn overlays for each brain at each injection site and histological images from a representative triple labelled brain.

Mediodorsal nucleus: ALO, PLO and PVO, each exhibit distinct connectivity patterns with the mediodorsal (MD) and submedius (Sub) nuclei of the thalamus. In relation to MD (Figure 5-A left, Figure 7), ALO receives strongest projections from the lateral part (MDl), particularly its most ventral portion. PLO receives strong projections from both the medial (MDm) and central

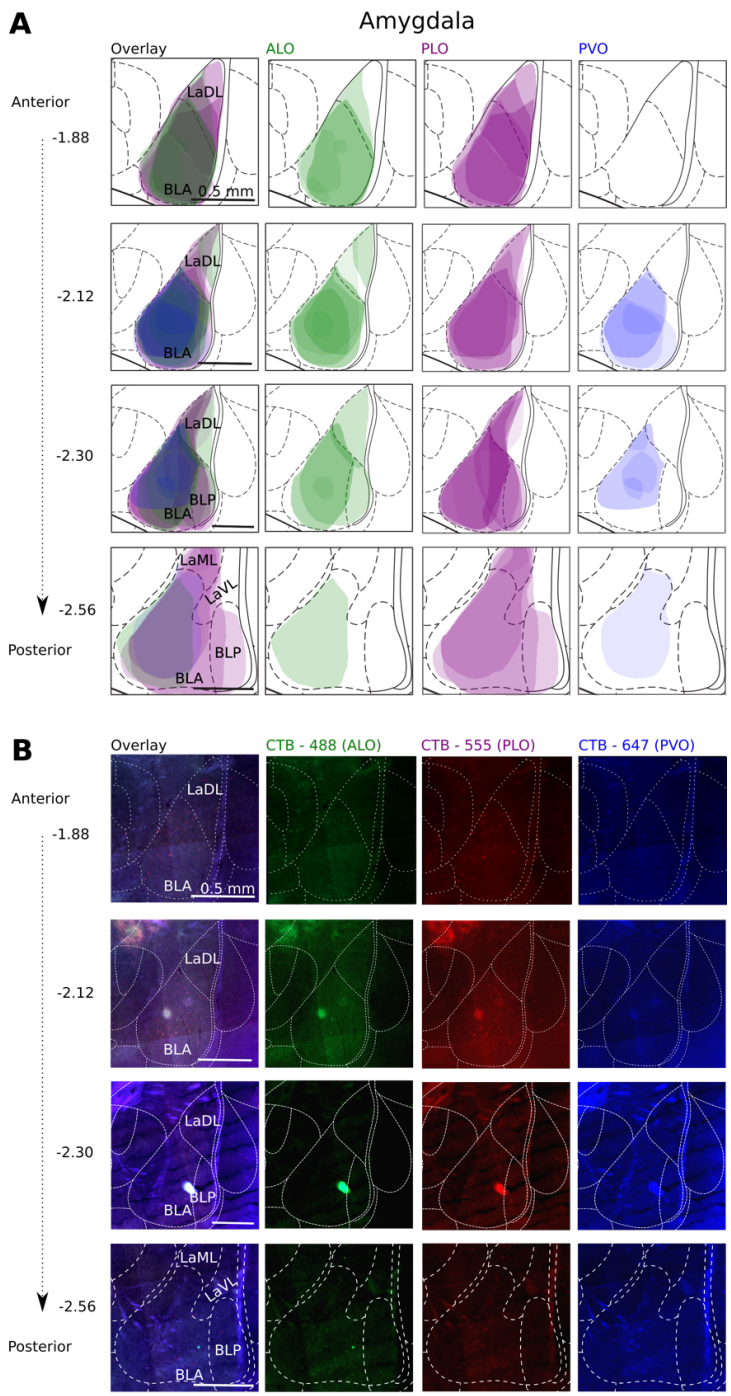

Figure 3. **Localisation and density of retrogradely-labelled cells in the amygdala, following CTB injection into ALO, PLO or PVO.** (A) Shaded areas correspond to superimposed hand drawings of the labelling in each brain included in the analysis, using an opacity value proportional to the labelling density level. *n* ALO = 6, *n* PLO = 5, *n* PVO = 4 injections. (B) Micrographs from representative brain with successful triple labelling. CTB: cholera toxin subunit B; ALO: orbitofrontal cortex, anterior lateral area; PLO: orbitofrontal cortex, posterior lateral area; PVO: orbitofrontal cortex, posterior lateral area; BLA: basolateral amygdala, anterior part ; BLP: basolateral amygdala, posterior part; LaDL: lateral amygdala, dorsolateral part; LaML: lateral amygdala, mediolateral part; LaVL, lateral amygdala, ventrolateral part.

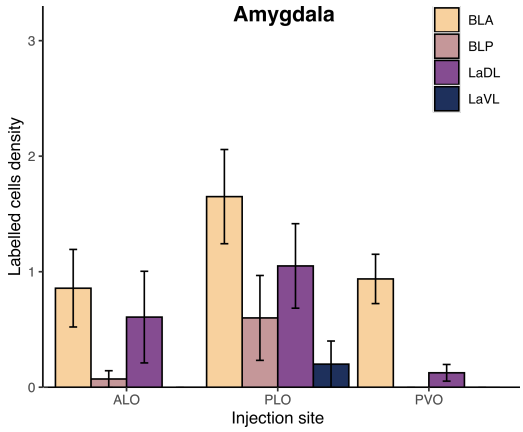

Figure 4. **Density of retrogradely-labelled cells in the amygdala following injection of CTB into ALO, PLO or PVO.** Average density across coronal slices -1.88, -2.12, -2.30 and -2.56 mm from Bregma. *n* ALO = 6, *n* PLO = 5, *n* PVO = 4 injections. Represented is the mean ± SEM. CTB: cholera toxin subunit B; ALO: orbitofrontal cortex, anterior lateral area; PLO: orbitofrontal cortex, posterior lateral area; PVO: orbitofrontal cortex, posterior lateral area; BLA: basolateral amygdala, anterior part; BLP: basolateral amygdala, posterior part; LaDL: lateral amygdala, dorsolateral part; LaML: lateral amygdala, mediolateral part; LaVL, lateral amygdala, ventrolateral part.

(MDc) parts of the medial dorsal thalamic nucleus, and only weak ones from MDl. In contrast, PVO receives only light projections from either lateral, medial or central MD.

Submedius nucleus: All portions of Sub project to every region of the OFC here investigated, although there is a clear spatial segregation in relation to where in Sub the strongest projections originate (Figure 6-A centre, Figure 6-B, Figure 7). ALO receives strongest projections from the posterior part of the dorsal submedius nucleus (SubD). In contrast, most afferents from Sub to PLO come from the ventral portion (SubV). On the other hand, PVO receives most Sub projections from the most anterior half, prominently from the dorsal portion, and slightly less from the ventral part.

Paratenial nucleus: The paratenial thalamic nucleus (PT; Figure 5) consistently exhibited moderate labelling following PLO injection but very light to no labelling with injections into ALO or PVO.

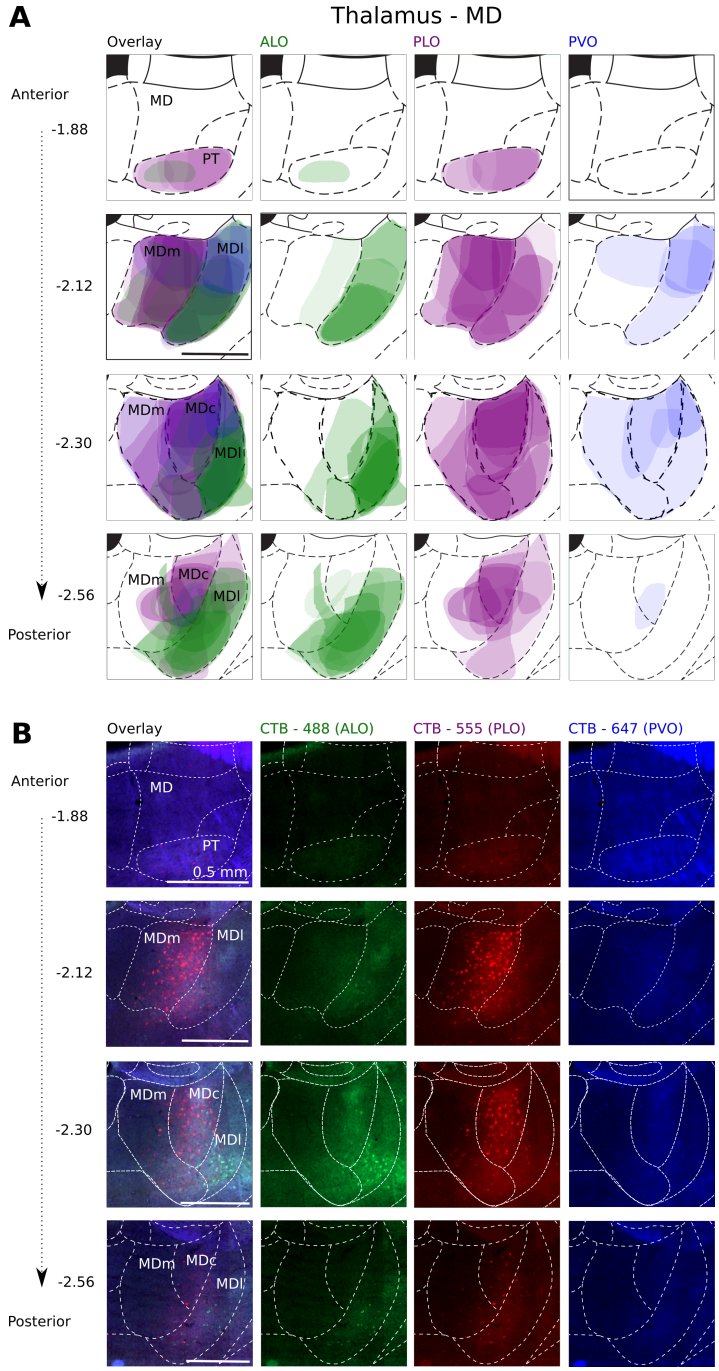

Figure 5. **Localisation and density of retrogradely-labelled cells in the mediodorsal (MD) thalamus, following CTB injection into ALO, PLO or PVO.** (A) Shaded areas correspond to superimposed hand drawings of the labelling in each brain included in the analysis, using an opacity value proportional to the labelling density level. *n* ALO = 6, *n* PLO = 5, *n* PVO = 4 injections. (B) Micrographs from representative brain with successful triple labelling. c: central; l: lateral; m: medial; CTB: cholera toxin subunit B; ALO: orbitofrontal cortex, anterior lateral area; PLO: orbitofrontal cortex, posterior lateral area; PVO: orbitofrontal cortex, posterior lateral area.

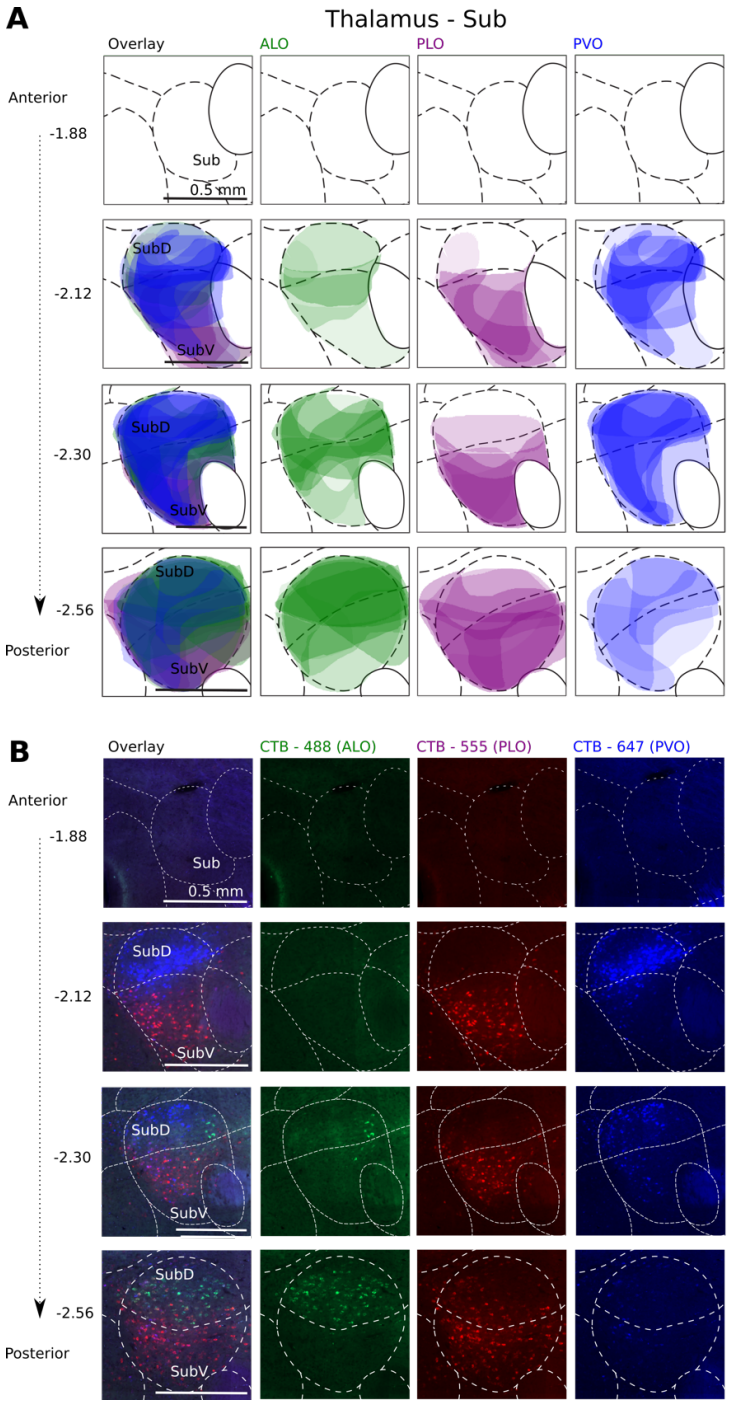

Figure 6. **Localisation and density of retrogradely-labelled cells in the submedius (Sub) nucleus of the thalamus, following CTB injection into ALO, PLO or PVO.** (A) Shaded areas correspond to superimposed hand drawings of the labelling in each brain included in the analysis, using an opacity value proportional to the labelling density level. *n* ALO = 6, *n* PLO = 5, *n* PVO = 4 injections. (B) Micrographs from representative brain with successful triple labelling. D: dorsal; V: ventral; CTB: cholera toxin subunit B; ALO: orbitofrontal cortex, anterior lateral area; PLO: orbitofrontal cortex, posterior lateral area; PVO: orbitofrontal cortex, posterior lateral area.

Nucleus reuniens: In the reuniens thalamic (Re) nucleus, we observed light labelling following tracer injections into both lateral and ventral posterior OFC, but mostly absent after injections into ALO (Figure 2).

In sum, the thalamus sends distinct and topographically organised projections from MD and Sub into ALO, PLO and PVO. Here, the anterior-posterior distinction between ALO and PLO is as clear and differentiated as the medial-lateral distinction between PLO and PVO. Projections from Re to PLO and PVO but not to ALO, reinforce the anterior-posterior distinction within LO. Labelling in PT after PLO injection but not after ALO or PVO also reinforces this anterior-posterior distinction within LO as well as a medial-lateral distinction between PLO and PVO.

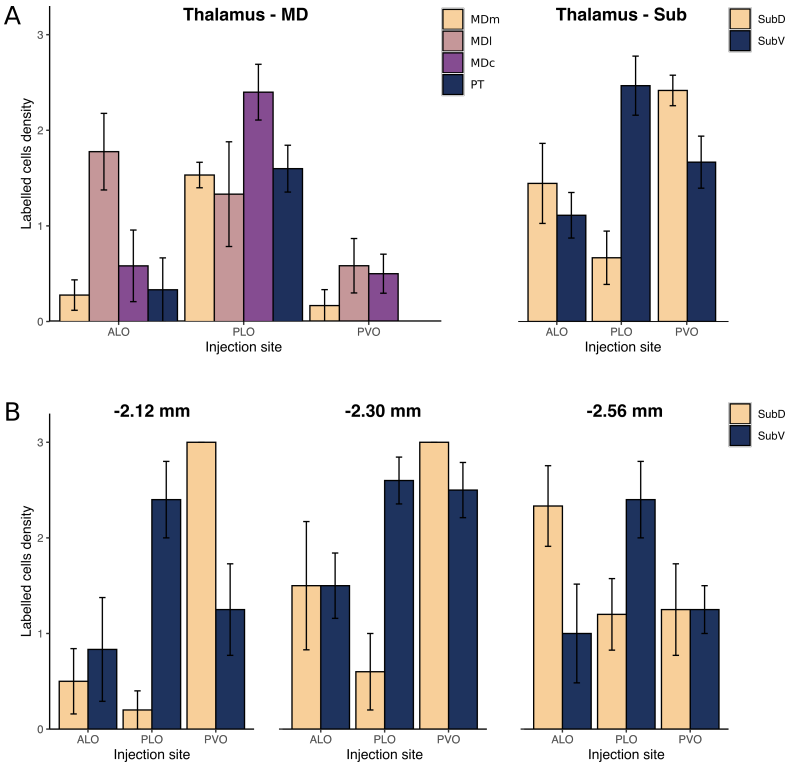

Figure 7. **Density of retrogradely-labelled cells in the mediodorsal and submedius nuclei of the thalamus following injection of CTB into ALO, PLO or PVO.** (A) Average density across coronal slices -1.88, -2.12, -2.30 and -2.56 mm from Bregma. (B) Average density of labelled cells in the submedius nucleus of the thalamus at -2.12, -2.30 and -2.56 mm from Bregma. *n* ALO = 6, *n* PLO = 5, *n* PVO = 4 injections. Represented is the mean ± SEM. c : central; l: lateral; m: medial; D: dorsal; V: ventral; CTB: cholera toxin subunit B; ALO: orbitofrontal cortex, anterior lateral area; PLO: orbitofrontal cortex, posterior lateral area; PVO: orbitofrontal cortex, posterior lateral

Table 2

Density of labelling in key areas observed following CTB injection into ALO, PLO or PVO

Structures	ALO	PLO	PVO
Prefrontal cortex			
orbitofrontal cortex, MO	-	+	+
prelimbic cortex	-	+	+
infralimbic cortex	-	+	+
anterior cingulate cortex, area 1	-	-	+
motor cortex	++	-	+
Sensory cortices			
gustatory cortex	+	+	+
piriform cortex	++	++	++
primary somatosensory cortex			
barrel cortex	+	-	++
forelimb, hindlimb & trunk areas	-	-	+
secondary visual cortex			
lateral area, mediolateral & mediomedial areas	-	-	+
auditory cortex	-	-	-
Thalamic nuclei			
mediodorsal			
medial part	+	++	-
central part	+	++	+
lateral part	++	+	+
submedius			
anterior section (-2.12)*			
dorsal part	+	-	++
ventral part	+	++	+
middle section (-2.30)*			
dorsal part	++	+	+++
ventral part	++	+++	+++
posterior section (-2.56)*			
dorsal part	++	+	+
ventral part	+	++	+
paratenial	-	++	-
reuniens	-	+	+
Amygdala			
basolateral			
anterior part	+	++	+
posterior part	-	+	-
lateral	-	+	-

Note. Only regions where main differences and relevant similarities were observed are represented. Because we observed no consistent differences in labelling density between the anterior and posterior portions of MO, here we collapsed its average labelling across all coronal slices. -, absence of labelling; +, weak labelling; ++, moderate labelling; +++, strong labelling; *, distance from Bregma in mm; CTB: cholera toxin subunit B.

Discussion

Here, we tested the hypothesis that OFC functional heterogeneity predicts meaningful differences in connectivity by simultaneously characterising the patterns of inputs of the anterior and posterior portions of LO, which have been previously found to be functional distinct (Panayi & Killcross, 2018). We also assessed whether any differences in connectivity between these two OFC subdivisions, ALO and PLO, are gradients in inputs strength or topographic organisation, or actual dissociations. Additionally, we contrast the input patterns into ALO and PVO with those into PVO, an anatomically adjacent OFC portion which is thought to be functionally distinct (Balleine et al., 2011; Corwin et al., 1994). Our approach allowed us to assess the extent of overlap, convergence and divergence between the projections of these OFC subdivisions, and thus define their topographic relationships. By using the same tracer to compare the connectivity across the subdivisions, we minimised potential interpretation problems caused by variability in uptake or transport by the cells, spread in the tissue or extent of local necrosis.

Our neuroanatomical characterisation revealed significant differences in cortical and sub-cortical inputs ALO, PLO and PVO. Yet, rather than completely distinct projection patterns, we mainly identified differences in the topographic organisation and in the gradation of connectivity strength into the OFC subdivisions investigated. Such differences were observed in the inputs from the medial prefrontal cortex, motor cortices, sensory cortices, amygdala and thalamus (Figure 8). We also considered other brain regions in our analysis, including entorhinal and perirhinal cortices; however, we did not find consistent and significant differences in their projections (see Figures S1, S2, S3).

Distinct and topographically organised thalamic inputs to OFC subdivisions

Thalamo-cortical connectivity has historically been one of the key criteria used to both segregate cortical regions and define functional circuits (Alexander, 1986; Rose & Woolsey,

1948). Medial, lateral and central nuclei of the MD thalamus receive partially overlapping but distinct subcortical afferents (Groenewegen, 1988). In our study, retrogradely-labelled cells in MD thalamus showed a notably separate pattern of projections between ALO, PLO and PVO. In fact, the distinction between ALO and PLO was as clear as the current medial-lateral OFC distinction between PLO and PVO.

The submedius nucleus of the thalamus shares strong reciprocal connections with the OFC, especially with VO/LO (Alcaraz et al., 2015; Coffield, Bowen, & Miletic, 1992; Kuramoto et al., 2017; Reep, Corwin, & King, 1996; Yoshida, Dostrovsky, & Chiang, 1992). In our tracing study, the most pronounced labelling in the brain of all subjects was seen in this area, with all portions of this thalamic nucleus projecting to every region of the OFC that we investigated (Figures 6, 7). Again, rather than a uniform connectivity pattern, we observed clear spatial segregation in relation to where in the Sub the strongest projections originate. Our results revealed that PVO receives most Sub projections from the most anterior half of the Sub, especially from the dorsal portion, and slightly less from the ventral part. Intriguingly, results from previous tracing studies (Kuramoto et al., 2017; Reep et al., 1996) revealed that the anterior portion of the ventral OFC receives inputs from SubV, suggesting a potential anterior-posterior distinction might also be present within ventral OFC.

The distinct medial-lateral gradient of OFC inputs from Sub we observed has been previously reported (Alcaraz et al., 2015; Reep et al., 1996). However, we also identified a novel pattern of Sub anterior-posterior projections which provides the clearest evidence of a distinction in afferents across the three OFC subregions we investigated in our study: ALO, PLO and PVO. In addition to these OFC subdivisions already mentioned, Sub also sends projections to MO (Kuramoto et al., 2017; Yoshida et al., 1992). Most of the double- or triple-labelled cells we observed were present in the Sub and it has previously reported there are neurons in this region that simultaneously project to lateral and ventral OFC, potentially linking

their functions under certain conditions (Kuramoto et al., 2017). While little is known about the function of this thalamic nucleus, recent studies have explored the functional significance of its connectivity with the OFC, revealing that an intact Sub is necessary for updating both stimulus-outcome (Alcaraz et al., 2015) and action-outcome associations (Fresno, Parkes, Faugère, Coutureau, & Wolff, 2019).

Multisensory nature of OFC inputs

The lateral orbital network, comprised of VO, LO and AI, is sometimes also referred to as a sensory network because of its strong multi-modal sensory (Carmichael & Price, 1995; Price, 2007). Here, we observed evidence of multi-sensory inputs into PVO. This in agreement with the attentional account of VO proposed by Hoover & Vertes (2011) and the connectivity described by Corwin & Reep (1998), showing that VO receives direct visual and somatosensory but not auditory information. By contrast, primary sensory inputs, other than gustatory and olfactory, into both ALO and PLO are sparse or mostly absent. Together these results highlight a medial-lateral distinction in the diversity of sensory inputs into LO and VO, raising the question of whether VO and LO are both part of the sensory network. Additionally, it puts into perspective the frequently used assertion that the OFC receives multi-modal sensory input. While this is true when the OFC is considered as a whole, the diversity and strength of primary sensory inputs varies depending on the subdivisions being studied. This emphasises the importance of specifying the portion of the OFC that is being studied and which specific functions are being attributed to it.

Amygdala input patterns into OFC subdivisions

OFC function has been closely linked to that of the amygdala, in particular its basolateral nucleus. Both OFC and BLA have been implicated in processes that support outcome-guided behaviour through associative learning of sensory-specific representations and predictive-cues.

Moreover, lesions of either region impair performance on outcome devaluation and reversal learning tasks (for reviews see Balleine & Killcross, 2006; Sharpe & Schoenbaum, 2016). OFC and BLA share strong reciprocal connections and their projections are topographically organised on both directions (Mcdonald, 1991; Mcdonald, 1998; Reep et al., 1996). In our tracing experiments, amygdala labelled cells were most prevalent in anterior BLA and following injection into PLO. By contrast, we observed only weak labelling after either ALO or PVO injections. This medial-lateral difference is consistent with the results obtained by Kita & Kitai (1990) following injections of anterograde tracer into anterior BLA: dense labelling in posterior lateral but not in ventral OFC.

The amygdala has been implicated in reversal learning, specifically in tracking previous outcomes and comparing them to current outcomes (Izquierdo et al., 2013; Lichtenberg et al., 2017; Schoenbaum, Setlow, Saddoris, & Gallagher, 2003; Stalnaker, Franz, Singh, & Schoenbaum, 2007). In particular, the dense BLA to PLO projections we observed here have been found to be necessary for using cue-generated reward expectations to guide decision making (Lichtenberg et al., 2017). Our results are also consistent with functional differences between ALO and PLO lesions, with posterior but not anterior LO lesions disrupting reversal learning (Panayi & Killcross, 2018). Furthermore, strong inputs from BLA to posterior but not to anterior OFC have been previously observed in primates (Freese & Amaral, 2009). This reinforces the idea, which had been previously hinted at by functional studies (Murray, Moylan, Saleem, Basile, & Turchi, 2015; Panayi & Killcross, 2018), of similar functional organisation principles between rodent and primate OFC subdivisions when functional differences along the anterior-posterior axis are considered.

Anterior and posterior LO are part of distinct anatomical and functional circuits

While PVO and PLO both receive sparse projections from regions along the medial wall, including IL, PL and MO (Figure 2; Table 2), such projections are very sparse and mostly

absent following injection into ALO. This is consistent with previous reports studying inputs from PL and IL to the OFC, which also suggest an anterior-posterior difference (Takagishi & Chiba, 1991; Vertes, 2004). Even though PVO and PLO injections were in the same anteroposterior plane and PVO is situated more medially, there was surprisingly little labelling along the medial wall following PVO injection. This argues against issues with polysynaptic labelling or tracer spreading within the OFC, especially between PVO and PLO injections. Indeed, we observed that CTB deposits that extended into adjacent AI produced a clearly distinct pattern of inputs to the adjacent PLO, with dense innervation from PL, MO and BLA (see Figure S5; consistent with Murphy & Deutch, 2018; Reep et al., 1996).

A number of studies have proposed a functional dissociation between OFC and PL in supporting Pavlovian and instrumental conditioning, respectively (Balleine & Dickinson, 1998; Corbit & Balleine, 2003; Ostlund & Balleine, 2005; Ostlund & Balleine, 2007). Both PL and OFC share strong reciprocal connections with the BLA (Mcdonald, 1991; Mcdonald, 1998), which in turn has been shown to play a role in both Pavlovian and instrumental outcome-mediated decision making (Balleine & Killcross, 2006; Johnson, Gallagher, & Holland, 2009). Therefore, the similar distinction in the density of projections from PL and BLA to anterior and posterior LO, suggest that BLA→PLO and PL→PLO might form a functional circuit involved in assessing the motivational significance of actions and stimuli, respectively.

We observed distinct labelling patterns following ALO and PLO injections also in the paratenial thalamic nucleus, which consistently exhibited moderate labelling following PLO injection but very light to no labelling with injections into ALO (Figure 2). Following injections of anterograde tracer into PT, Vertes & Hoover (2008) observed a similar distinction in its projections to the anterior and posterior portions of LO, with moderate labelling in the PLO but only very sparse in ALO. However, while they observed projections from PT to PVO, we saw no retrogradely-labelled cells in PT following injection into PVO. Further

investigations may be necessary to understand this difference. Although the function of this thalamic nucleus is uncertain, its inputs from the hypothalamus, brain stem and limbic system suggest it might play a role in goal-directed behaviour, facilitating action selection in changing environments by conveying multimodal information (Vertes & Hoover, 2008). Thus, the distinct projection patterns from PT to anterior and posterior LO is consistent with the functional differences observed by Panayi & Killcross (2018) suggesting that posterior but not anterior LO is critical for updating the value of expected outcomes.

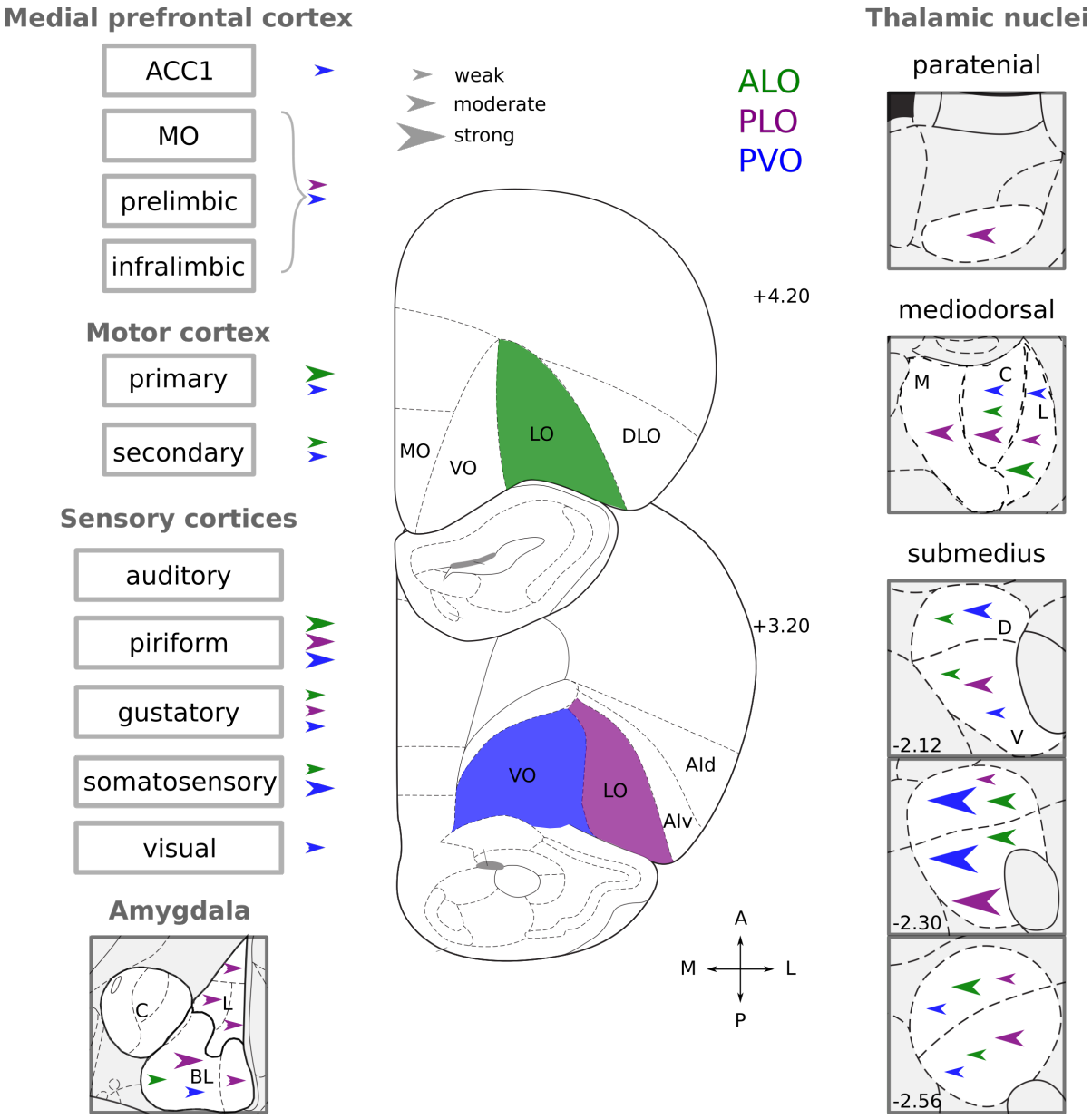

Figure 8. **Density of key inputs into ALO, PLO and PVO.** The different arrow sizes represent the relative average density of retrogradely-labelled cells following CTB injection (i.e. weak, moderate or strong). Panels depicting labelling in amygdala and in MD thalamus represent the average density labelling in all slices quantified and not at that particular coronal section. ACC1: anterior cingulate cortex, area 1; AId: agranular insular cortex, dorsal part; AIv: agranular insular cortex, ventral part; ALO: anterior lateral OFC; CTB: cholera toxin subunit B; DLO: dorsolateral OFC; IL: infralimbic cortex; LO: lateral OFC; M1: primary motor cortex; M2: secondary motor cortex; MO: medial OFC; PL: prelimbic cortex; PLO: posterior lateral OFC; PVO: posterior ventral OFC; VO: ventral OFC; A: anterior; P: posterior; BL: basolateral; C: central; M: medial; L: lateral; D: dorsal; V: ventral.

Putting it all together

Even very functionally distinct brain regions often show substantial overlap in their inputs and outputs (Passingham, Stephan, & Kötter, 2002). It is, thus, not surprising that different portions of the OFC show the graded connectivity patterns we described here. It might, therefore, be useful to consider the question of what makes two adjacent regions distinct. We believe that integrating neuroanatomical characterisation with functional differences is essential. For instance, ventral and lateral OFC are generally considered separate regions (Krettek & Price, 1977; Price, 2006; Ray & Price, 1992). This distinction is supported by functional dissociations (e.g. Balleine et al., 2011) and differences in efferent (e.g. Schilman, Uylings, Graaf, Joel, & Groenewegen, 2008) and afferent (Table 2) projections.

In light of this standard distinction between ventral and lateral OFC, we ought to consider a division between the anterior and posterior portions of LO. A functional dissociation between ALO and PLO has been previously reported (Panayi & Killcross, 2018) and our neuroanatomical characterisation of their inputs has shed light on the circuitry underlying those differences. We observed a similar degree of distinction between the afferent projections into ALO and PLO and the projections into PLO and PVO. Thus, while further studies might be necessary, the evidence so far firmly supports a distinction along the anterior-posterior axis of LO. We did not explore whether a similar division might exist within VO. However, the projection patterns we observed in the submedius nucleus of the thalamus following injection into posterior VO differ substantially from those seen by Kuramoto and colleagues (2017) following injection of the same retrograde tracer into the anterior VO.

Our results revealed that different portions of the Sub send a distinct, strong and topographically organised projections to OFC subdivisions. Thus, the Sub presents itself as a key anatomical area within the thalamus whose projections may allow the distinction of orbital subregions more effectively than those of the MD thalamus, which have traditionally been used

when defining prefrontal circuits (Rose & Woolsey, 1948). The specific pattern and relative density of anatomical projections between brain regions is also one of the criteria used to establish homology between cortical areas of different species (Rose & Woolsey, 1948; Uylings, Groenewegen, & Kolb, 2003). A detailed understanding of the anatomy of OFC subdivisions will, therefore, allow for connectivity-based inferences on cross species-homologies. Thus, further anatomical and functional characterisation of contained OFC subregions will likely be key to establish clearer homologies between rodent and primate OFC.

Funding: This work was supported by a Biotechnology and Biological Sciences Research Council Doctoral Training Partnership studentship awarded to I.V.B. and by a Wellcome trust Senior Research Fellowship awarded to M. E. Walton (202831/Z/16/Z).

Authors contributions: MCP and MEW conceived the project. IVB and MCP conducted the experiments. IVB analysed the data, with input from MCP and MEW. IVB, MCP and MEW wrote the paper.

Competing interests: The authors declare no competing interest.

References

Alcaraz, F., Marchand, A. R., Vidal, E., Guillou, A., Faugère, A., Coutureau, E., & Wolff, M. (2015). Flexible use of predictive cues beyond the orbitofrontal cortex: Role of the submedius thalamic nucleus. *Journal of Neuroscience*, *35*(38), 13183–13193. https://doi.org/10.1523/JNEUROSCI.1237-15.2015

Alexander, G. (1986). Parallel Organization of Functionally Segregated Circuits Linking Basal Ganglia and Cortex. *Annual Review of Neuroscience*, *9*(1), 357–381. https://doi.org/10.1146/annurev.neuro.9.1.357

Balleine, B. W., & Dickinson, A. (1998). Goal-directed instrumental action: Contingency and incentive learning and their cortical substrates. *Neuropharmacology*, *37*(4–5), 407–419. https://doi.org/10.1016/S0028-3908(98)00033-1

Balleine, B. W., & Killcross, S. (2006). Parallel incentive processing: an integrated view of amygdala function. *Trends in Neurosciences*, *29*(5), 272–279. https://doi.org/10.1016/j.tins.2006.03.002

Balleine, B. W., Leung, B. K., & Ostlund, S. B. (2011). The orbitofrontal cortex, predicted value, and choice. *Annals of the New York Academy of Sciences*, *1239*(1), 43–50. https://doi.org/10.1111/j.1749-6632.2011.06270.x

Barreiros, I. V., Ishii, H., Walton, M. E., & Panayi, M. C. (2020). Defining an orbitofrontal compass: functional and anatomical heterogeneity across anterior-posterior and medial-lateral axes. *Submitted*.

Bradfield, L. A., & Hart, G. (2020). Rodent medial and lateral orbitofrontal cortices represent unique components of cognitive maps of task space. *Neuroscience and Biobehavioral Reviews*, *108*(November 2019), 287–294. https://doi.org/10.1016/j.neubiorev.2019.11.009

Bradfield, L. A., Hart, G., & Balleine, B. W. (2018). Inferring action-dependent outcome representations depends on anterior but not posterior medial orbitofrontal cortex. *Neurobiology of Learning and Memory*, *155*(August), 463–473. https://doi.org/10.1016/j.nlm.2018.09.008

Carmichael, S. T., & Price, J. L. (1995). Limbic connections of the orbital and medial prefrontal cortex in macaque monkeys. *Journal of Comparative Neurology*, *363*(4), 615–641. https://doi.org/10.1002/cne.903630408

Coffield, J. A., Bowen, K. K., & Miletic, V. (1992). Retrograde tracing of projections between the nucleus submedius, the ventrolateral orbital cortex, and the midbrain in the rat. *Journal of Comparative Neurology*, *321*(3), 488–499. https://doi.org/10.1002/cne.903210314

Conte, W. L., Kamishina, H., & Reep, R. L. (2009). Multiple neuroanatomical tract-tracing using fluorescent Alexa Fluor conjugates of cholera toxin subunit B in rats. *Nature Protocols*, *4*(8), 1157–1166. https://doi.org/10.1038/nprot.2009.93

Corbit, L. H., & Balleine, B. W. (2003). The role of prelimbic cortex in instrumental conditioning. *Behavioural Brain Research*, *146*(1–2), 145–157. https://doi.org/10.1016/j.bbr.2003.09.023

Corwin, J. V., Fussinger, M., Meyer, R. C., King, V. R., & Reep, R. L. (1994). Bilateral destruction of the ventrolateral orbital cortex produces allocentric but not egocentric spatial deficits in rats. *Behavioural Brain Research*, *61*(1), 79–86. https://doi.org/10.1016/0166-4328(94)90010-8

Corwin, J. V., & Reep, R. L. (1998). Rodent posterior parietal cortex as a component of a cortical network mediating directed spatial attention. *Psychobiology*, *26*(2), 87–102. https://doi.org/10.3758/BF03330596

Freese, J. L., & Amaral, D. G. (2009). Neuroanatomy of the Primate Amygdala. In *The Human Amygdala*.

Fresno, V., Parkes, S. L., Faugère, A., Coutureau, E., & Wolff, M. (2019). A thalamocortical circuit for updating action-outcome associations. *ELife*, *8*, 1–13. https://doi.org/10.7554/eLife.46187

Groenewegen, H. J. (1988). Organization of the afferent connections of the mediodorsal thalamic nucleus in the rat, related to the mediodorsal-prefrontal topography. *Neuroscience*, *24*(2), 379–431. https://doi.org/10.1016/0306-4522(88)90339-9

Hoover, W. B., & Vertes, R. P. (2011). Projections of the medial orbital and ventral orbital cortex in the rat. *Journal of Comparative Neurology*, *519*(18), 3766–3801. https://doi.org/10.1002/cne.22733

Izquierdo, A. (2017). Functional heterogeneity within rat orbitofrontal cortex in reward learning and decision making. *Journal of Neuroscience*, *37*(44), 10529–10540. https://doi.org/10.1523/JNEUROSCI.1678-17.2017

Izquierdo, A., Darling, C., Manos, N., Pozos, H., Kim, C., Ostrander, S., … Rudebeck, P. H. (2013). Basolateral amygdala lesions facilitate reward choices after negative feedback in rats. *Journal of Neuroscience*, *33*(9), 4105–4109. https://doi.org/10.1523/JNEUROSCI.4942-12.2013

Johnson, A. W., Gallagher, M., & Holland, P. C. (2009). The basolateral amygdala is critical to the expression of pavlovian and instrumental outcome-specific reinforcer devaluation effects. *Journal of Neuroscience*. https://doi.org/10.1523/JNEUROSCI.3758-08.2009

Kita, H., & Kitai, S. T. (1990). Amygdaloid projections to the frontal cortex and the striatum in the rat. *Journal of Comparative Neurology*, *298*(1), 40–49. https://doi.org/10.1002/cne.902980104

Krettek, J. E., & Price, J. L. (1977a). Projections from the amygdaloid complex to the cerebral cortex and thalamus in the rat and cat. *Journal of Comparative Neurology*, *172*(4), 687–722. https://doi.org/10.1002/cne.901720408

Krettek, J. E., & Price, J. L. (1977b). The cortical projections of the mediodorsal nucleus and adjacent thalamic nuclei in the rat. *Journal of Comparative Neurology*. https://doi.org/10.1002/cne.901710204

Kuramoto, E., Iwai, H., Yamanaka, A., Ohno, S., Seki, H., Tanaka, Y. R., … Goto, T. (2017). Dorsal and ventral parts of thalamic nucleus submedius project to different areas of rat orbitofrontal cortex: A single neuron-tracing study using virus vectors. *Journal of Comparative Neurology*, *525*(18), 3821–3839. https://doi.org/10.1002/cne.24306

Lichtenberg, N. T., Pennington, Z. T., Holley, S. M., Greenfield, V. Y., Cepeda, C., Levine, M. S., & Wassum, K. M. (2017). Basolateral amygdala to orbitofrontal cortex projections enable cue-triggered reward expectations. *Journal of Neuroscience*, *37*(35). https://doi.org/10.1523/JNEUROSCI.0486-17.2017

Mcdonald, A. J. (1991). Organization of amygdaloid projections to the prefrontal cortex and associated striatum in the rat. *Neuroscience*, *44*(1), 1–14. https://doi.org/10.1016/0306-4522(91)90247-L

Mcdonald, Alexander J. (1998). Cortical pathways to the mammalian amygdala. *Progress in Neurobiology*, *55*(3), 257–332. https://doi.org/10.1016/S0301-0082(98)00003-3

Murphy, M. J. M., & Deutch, A. Y. (2018). Organization of afferents to the orbitofrontal cortex in the rat. *Journal of Comparative Neurology*, *526*(9), 1498–1526. https://doi.org/10.1002/cne.24424

Murray, E. A., Moylan, E. J., Saleem, K. S., Basile, B. M., & Turchi, J. (2015). Specialized areas for value updating and goal selection in the primate orbitofrontal cortex. *ELife*, *4*(5), 1–18. https://doi.org/10.7554/eLife.11695

Ostlund, Scan B., & Balleine, B. W. (2005). Lesions of medial prefrontal cortex disrupt the acquisition but not the expression of goal-directed learning. *Journal of Neuroscience*, *25*(34), 7763–7770. https://doi.org/10.1523/JNEUROSCI.1921-05.2005

Ostlund, Sean B., & Balleine, B. W. (2007). Orbitofrontal cortex mediates outcome encoding in pavlovian but not instrumental conditioning. *Journal of Neuroscience*, *27*(18), 4819–4825. https://doi.org/10.1523/JNEUROSCI.5443-06.2007

Panayi, M. C., & Killcross, S. (2018). Functional heterogeneity within the rodent lateral orbitofrontal cortex dissociates outcome devaluation and reversal learning deficits. *ELife*, *7*, 1–27. https://doi.org/10.7554/eLife.37357.001

Passingham, R. E., Stephan, K. E., & Kötter, R. (2002). The anatomical basis of functional localization in the cortex. *Nature Reviews Neuroscience*, *3*(8), 606–616. https://doi.org/10.1038/nrn893

Paxinos, G., & Watson, C. (1998). The Rat Brain in Stereotaxic Coordinates. In *Elsevier Academic Press* (4th ed.).

Price, J. L. (2006). Architectonic structure of the orbital and medial prefrontal cortex. In *The Orbitofrontal Cortex*. https://doi.org/10.1093/acprof:oso/9780198565741.003.0001

Price, J. L. (2007). Definition of the Orbital Cortex in Relation to Specific Connections with Limbic and Visceral Structures and Other Cortical Regions. *Annals of the New York Academy of Sciences*, *1121*(1), 54–71. https://doi.org/10.1196/annals.1401.008

Ray, J. P., & Price, J. L. (1992). The organization of the thalamocortical connections of the mediodorsal thalamic nucleus in the rat, related to the ventral forebrain–prefrontal cortex topography. *Journal of Comparative Neurology*, *323*(2), 167–197. https://doi.org/10.1002/cne.903230204

Reep, R. L., Corwin, J. V., & King, V. (1996). Neuronal connections of orbital cortex in rats: Topography of cortical and thalamic afferents. *Experimental Brain Research*. https://doi.org/10.1007/BF00227299

Rose, J. E., & Woolsey, C. N. (1948). The orbitofrontal cortex and its connections with the mediodorsal nucleus in rabbit, sheep and cat. *Research Publications - Association for Research in Nervous and Mental Disease*.

Schilman, E. A., Uylings, H. B. M., Graaf, Y. G. de, Joel, D., & Groenewegen, H. J. (2008). The orbital cortex in rats topographically projects to central parts of the caudate-putamen complex. *Neuroscience Letters*, *432*(1), 40–45. https://doi.org/10.1016/j.neulet.2007.12.024

Schoenbaum, G., Setlow, B., Saddoris, M. P., & Gallagher, M. (2003). Encoding predicted outcome and acquired value in orbitofrontal cortex during cue sampling depends upon input from basolateral amygdala. *Neuron*, *39*(5), 855–867. https://doi.org/10.1016/S0896-6273(03)00474-4

Sharpe, M. J., & Schoenbaum, G. (2016). Back to basics: Making predictions in the orbitofrontal-amygdala circuit. *Neurobiology of Learning and Memory*, Vol. 131. https://doi.org/10.1016/j.nlm.2016.04.009

Stalnaker, T. A., Franz, T. M., Singh, T., & Schoenbaum, G. (2007). Basolateral Amygdala Lesions Abolish Orbitofrontal-Dependent Reversal Impairments. *Neuron*, *54*(1), 51–58. https://doi.org/10.1016/j.neuron.2007.02.014

Takagishi, M., & Chiba, T. (1991). Efferent projections of the infralimbic (area 25) region of the medial prefrontal cortex in the rat: an anterograde tracer PHA-L study. *Brain Research*, *566*(1–2), 26–39. https://doi.org/10.1016/0006-8993(91)91677-S

Uylings, H. B. M., Groenewegen, H. J., & Kolb, B. (2003). Do rats have a prefrontal cortex? *Behavioural Brain Research*, *146*(1–2), 3–17. https://doi.org/10.1016/j.bbr.2003.09.028

Van De Werd, H. J. J. M., & Uylings, H. B. M. (2008). The rat orbital and agranular insular prefrontal cortical areas: A cytoarchitectonic and chemoarchitectonic study. *Brain Structure and Function*, *212*(5), 387–401. https://doi.org/10.1007/s00429-007-0164-y

Vertes, R. P. (2004). Differential Projections of the Infralimbic and Prelimbic Cortex in the Rat. *Synapse*, *51*(1), 32–58. https://doi.org/10.1002/syn.10279

Vertes, R. P., & Hoover, W. B. (2008). Projections of the paraventricular and paratenial nuclei of the dorsal midline thalamus in the rat. *Journal of Comparative Neurology*, *508*(2), 212–237. https://doi.org/10.1002/cne.21679

Yoshida, A., Dostrovsky, J. O., & Chiang, C. Y. (1992). The afferent and efferent connections of the nucleus submedius in the rat. *Journal of Comparative Neurology*. https://doi.org/10.1002/cne.903240109

Supplemental material

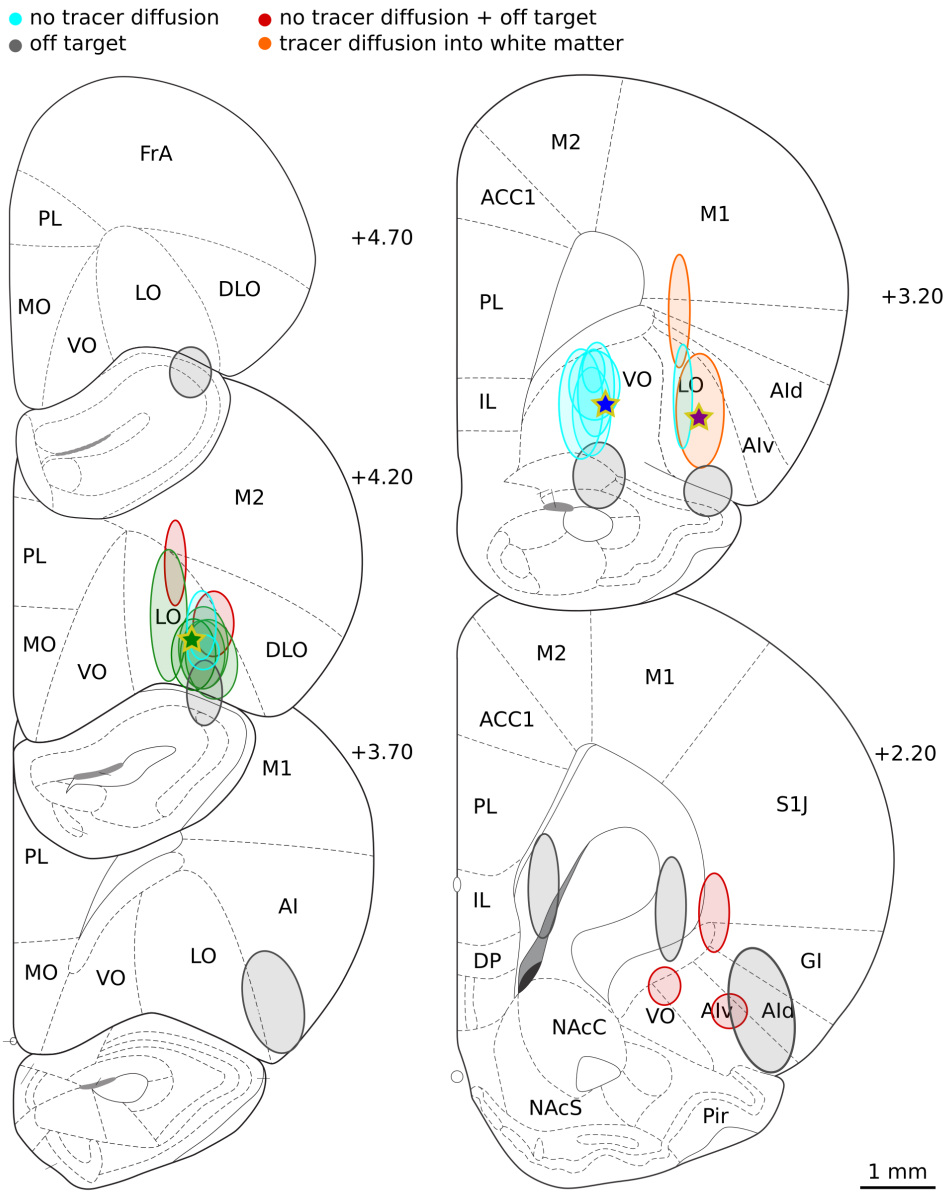

Figure S1. **Coronal sections depicting core of tracer deposits of excluded injections, illustrated at the level of maximal deposit.** Star and oval shapes represent the intended and the observed injection sites core, respectively. Data from injections that were off target (n = 11), in which tracer did not diffuse (n = 8), were both off target and the tracer did not diffuse (n = 6) or diffused into the white matter (n = 2) were excluded from all analyses. Two of the excluded injections were anterior to +4.70 mm from Bregma and are not represented here. Distances shown are distances from bregma in mm. MO: orbitofrontal cortex, medial area; VO: orbitofrontal cortex, ventral area; LO: orbitofrontal cortex, lateral area; DLO: orbitofrontal cortex, dorsolateral area; PL: prelimbic cortex; IL: infralimbic cortex; M1: primary motor cortex; M2: secondary motor cortex; ACC1: anterior cingulate cortex, area 1; AI: agranular insular cortex; AId: agranular insular cortex, dorsal part; AIv: agranular insular cortex, ventral part; FrA: frontal association cortex; GI: gustatory insular cortex; NAcC: nucleus accumbens, core; NAcS: nucleus accumbens, shell; DP: dorsal peduncular cortex; S1J: primary somatosensory cortex, jaw region; Pir: piriform cortex.

Table S1

Average labelling density observed following CTB injection into ALO, PLO or PVO

		Ipsilateral			Contralateral		
Structure	AP coordinate (mm)	ALO	PLO	PVO	ALO	PLO	PVO
Prefrontal cortex							
Orbitofrontal	+4.70	saturation	1.00	0	1.50	0.80	0
dorsolateral part	+4.70	saturation	1.00	0	1.50	0.80	0
	+4.20	0.67	0.60	0.25	0.33	0.80	0.25
lateral part	+4.70	saturation	1.40	1.25	2.17	1.40	1.25
	+4.20	saturation	1.25	2.00	2.83	2.20	1.75
	+3.70	saturation	saturation	saturation	2.67	2.80	2.50
	+3.20	2.33	saturation	2.50	2.33	2.80	1.75
	+2.70	2.00	saturation	2.25	1.67	1.40	1.50
medial part	+4.70	0.33	1.20	0.50	0.17	1.60	0.50
	+4.20	0.33	1.20	0.50	0.33	1.40	0.75
	+3.70	0	1.00	0.75	0	0.80	0.75
ventral part	+4.70	1.00	1.40	1.50	1.00	2.00	1.25
	+4.20	0.83	1.00	1.25	0.67	1.40	1.50
	+3.70	0.83	0.80	saturation	0.83	0.60	2.50
	+3.20	1.83	1.80	saturation	1.67	1.60	3.00
	+2.70	2.17	2.40	saturation	1.00	1.80	2.75
	+2.20	0	2.80	2.50	0	1.80	1.50
Infralimbic	+3.20	0	0.40	0.50	0	0.40	0.50
	+2.70	0	0.20	0.25	0	0.20	0
	+2.20	0	0.20	0.25	0	0	0
Prelimbic	+4.70	0	0.20	0	0	0.40	0
	+4.20	0	0.20	0.25	0	0.20	0.25
	+3.70	0	0.40	0.25	0	0.40	0.25
	+3.20	0	0.40	0.50	0	0.20	0.25
	+2.70	0.17	0	0.25	0.17	0	0.25
	+2.20	0	0	0	0	0	0.25
Cingulate, area 1	+3.70	0.17	0.20	0.50	0	0.20	0
	+3.20	0	0	0.75	0	0	0
	+2.70	0.17	0	0.25	0	0	0.25
	+2.20	0	0	0.25	0	0	0
Insular cortex							
Agranular insula	+3.70	0	saturation	0.20	0.17	0.80	0
	-1.88	0.67	0.40	0.50	0	0	0
	-2.12	0.83	0.40	0.25	0	0	0
	-2.30	0.67	0.60	0.75	0	0	0
	-2.56	0.50	0.60	0.25	0	0	0
dorsal part	+3.20	0	0.40	0	0.17	0.20	0
	+2.70	1.17	0.80	0.25	0.67	1.20	0
	+2.20	1.33	1.80	1.75	0.83	1.00	0
ventral part	+3.20	0.17	1.00	0	0.33	0.40	0
	+2.70	1.50	saturation	1.25	1.17	2.20	0.25
	+2.20	1.33	1.80	1.75	0.83	1.20	0.50
Gustatory insula	+2.70	0.17	0.40	0	0.17	0.20	0
	+2.20	0.33	0.60	0	0	0.20	0
	-1.88	0.83	0.40	0.50	0	0	0
	-2.12	0.17	1.20	1.50	0	0	0
	-2.30	0.83	1.00	1.75	0	0	0
	-2.56	0.83	0.80	1.25	0	0	0
Motor cortex							
Primary	+3.70	1.00	0.20	0.50	1.67	0.20	0.50
	+3.20	1.33	0	0.50	1.50	0	1.00
	+2.70	1.17	0	1.00	1.00	0	1.00
	+2.20	1.17	0	1.00	0.33	0	0
	-1.88	0.17	0.20	0.25	0	0	0
	-2.12	0	0	0.50	0	0	0
	-2.30	0	0	0	0	0	0
	-2.56	0	0	0.25	0	0	0
Secondary	+4.20	0.67	0.60	0.50	0.17	0.60	0.25
	+3.70	0.67	0.20	0.25	0.33	0	0.25
	+3.20	1.00	0.20	0.25	1.33	0.20	0.50
	+2.70	1.33	0.20	0.50	0.83	0	1.00
	+2.20	0.33	0	0.75	0.17	0	0.50
	-1.88	1.00	0	0.50	0	0	0.25
	-2.12	0	0	2.00	0	0	1.00
	-2.30	0	0	0.25	0	0	0
	-2.56	0	0	0	0	0	0
Sensory cortices							
Piriform	+3.70	1.50	1.20	2.75	0	0	0
	+3.20	2.17	1.80	2.75	0	0	0
	+2.70	2.17	2.00	3.00	0.14	0	0
	+2.20	2.33	2.20	0	0	0	0
	-1.88	0.17	0.80	0.75	0	0	
	-2.12	0	0.40	0.75	0	0	0

	-2.30	0	0.40	0.50	0	0	0
	-2.56	0.40	0.25	0	0	0	0
Somatosensory							
primary/barrel cortex	-1.88	0.50	0	0.75	0	0	0
	-2.12	0.33	0	2.25	0	0	0
	-2.30	0.33	0.40	1.75	0	0	0
	-2.56	0.33	0	1.50	0	0	0
forelimb and hindlimb regions	-1.88	0	0	0.50	0	0	0
	-2.12	0	0	0.50	0	0	0
trunk region	-2.30	0.17	0	0.50	0	0	0
	-2.56	0.17	0	0.50	0	0	0
secondary somatosensory	-1.88	0	0.20	0.25	0	0	0
	-2.12	0.40	0.20	1.50	0	0	0
	-2.30	0	0	0.50	0	0	0
	-2.56	0	0	0.25	0	0	0
Auditory							
primary	-5.30	0	0	0	0	0	0
secondary							
dorsal part	-5.30	0	0	0	0	0	0
ventral part	-5.30	0	0	0	0	0	0
Visual cortex							
primary							
binocular area	-5.30	0	0	0	0	0	0
monocular area	-5.30	0	0	1.00	0	0	0
secondary							
lateral area	-5.30	0.33	0	0.75	0	0	0
mediolateral area	-5.30	0.17	0	0.75	0	0	0
mediomedial area	-5.30	0.17	0	0.25	0	0	0
Temporal lobe							
Amygdala							
basolateral	-1.88	1.17	1.60	0.75	0	0	0
anterior part	-1.88	1.17	1.60	0.75	0	0	0
	-2.12	1.33	2.00	1.25	0	0	0
	-2.30	0.67	1.80	1.25	0	0	0
	-2.56	0.33	1.20	0.50	0	0	0
posterior part	-2.30	0	0.40	0	0	0	0
	-2.56	0	0.80	0	0	0	0
lateral							
dorsolateral part	-1.88	0.17	1.20	0.25	0	0	0
	-2.12	0.17	1.40	0	0	0	0
	-2.30	0.50	1.20	0.25	0	0	0
	-2.56	0.17	0.40	0	0	0	0
ventromedial part	-2.56	0	0.60	0	0	0	0
ventrolateral part	-2.56	0	0.20	0	0	0	0
Entorhinal cortex	-5.30	0.83	1.20	1.50	0	0	0.33
Perirhinal cortex	-5.30	0.17	0.40	0.75	0	0	0
Parietal lobe							
Retrosplenial cortex	-1.88	0.33	0	0	0	0	0
	-2.12	0	0	0	0	0	0
	-2.30	0.17	0	0.25	0	0	0
	-2.56	0	0	0	0	0	0
	-2.50	0	0	0.35	0	0	0
Thalamic nuclei							
Mediodorsal	-1.88	0	0	0	0	0	0
central part	-2.30	0.33	2.20	0.75	0	0	0
	-2.56	0.83	2.60	0.25	0	0	0
lateral part	-2.12	1.20	1.80	1.25	0	0	0
	-2.30	2.00	1.40	0.75	0	0	0
	-2.56	2.00	0.80	0	0	0	0
medial part	-2.12	0.20	2.60	0.25	0	0	0
	-2.30	0.17	1.60	0.25	0	0	0
	-2.56	0.50	0.40	0	0	0	0
Paratenial	-1.88	0.40	1.60	0	0	0	0
Reunens	-2.12	0	0.40	0.50	0	0	0
	-2.30	0.33	0.80	0.50	0	0	0
	-2.56	0.17	0.80	0.50	0	0	0
Submedius	-1.88	0	0	0	0	0	0
dorsal part	-2.12	0.60	0.20	2.25	0	0	0
	-2.30	1.50	0.60	3.00	0	0	0
	-2.56	2.33	1.20	1.25	0	0	0
ventral part	-2.12	0.60	2.40	1.25	0	0	0
	-2.30	1.50	2.60	2.50	0	0	0
	-2.56	1.00	2.40	1.25	0	0	0

Note. Average values were obtained following 4-level categorisation (0, absence of labelling; 1, weak; 2, moderate; 3, strong) of labelling density. Areas with saturated labelling, only found around injection sites, were not included in the analyses.

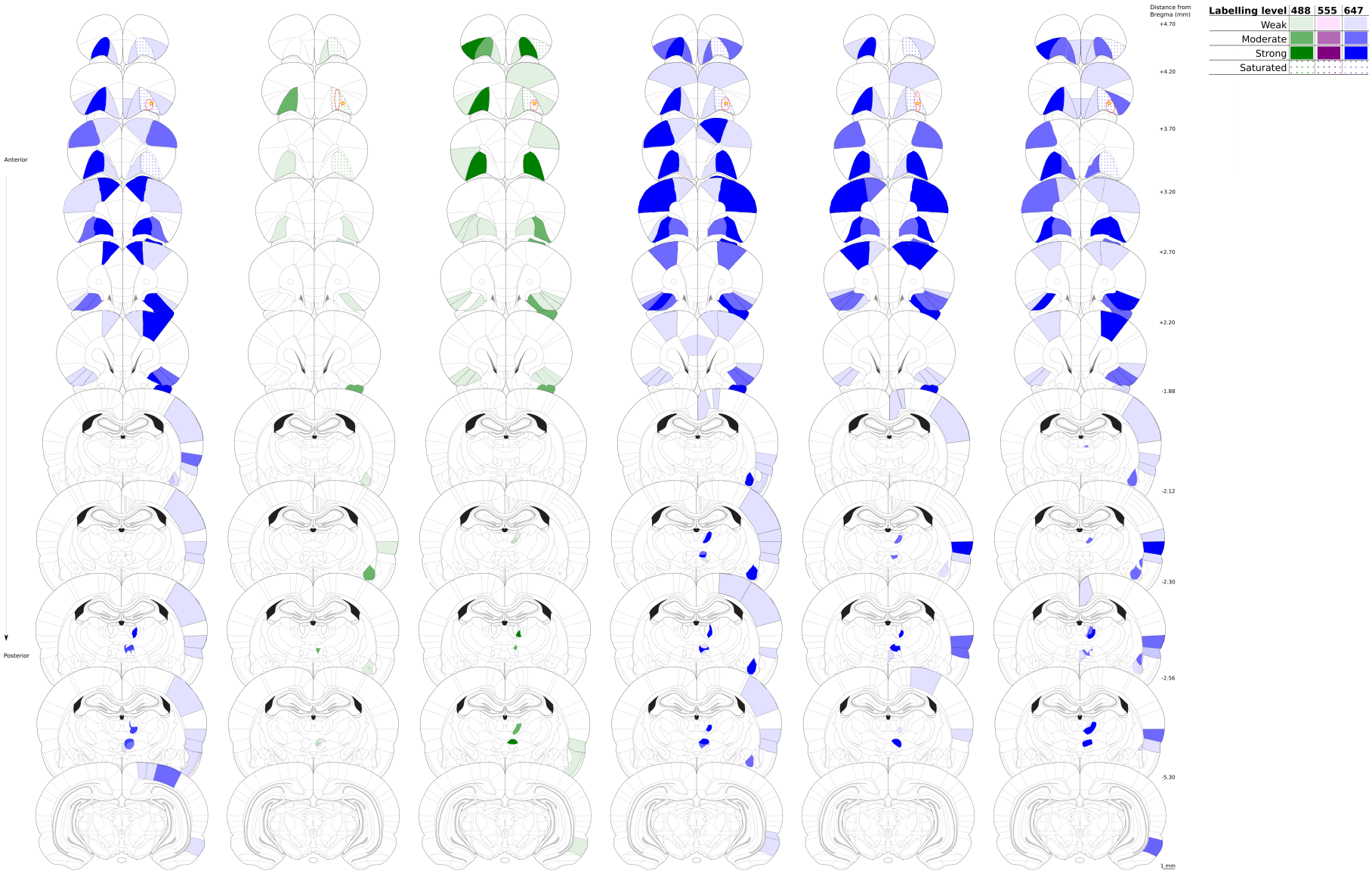

Figure S2. **Density of retrogradely-labelled cells following CTB injection into ALO.** Lighter or darker shades represent lower or higher labelling densities, respectively. Red star and oval shapes represent the intended and the observed injection sites core, respectively. Brains are sorted by the location of its observed injection site, from medial to lateral. CTB: cholera toxin subunit B; ALO: orbitofrontal cortex, anterior lateral area; 488: Alexa Fluor 488; 555: Alexa Fluor 555; 647: Alexa Fluor 647.

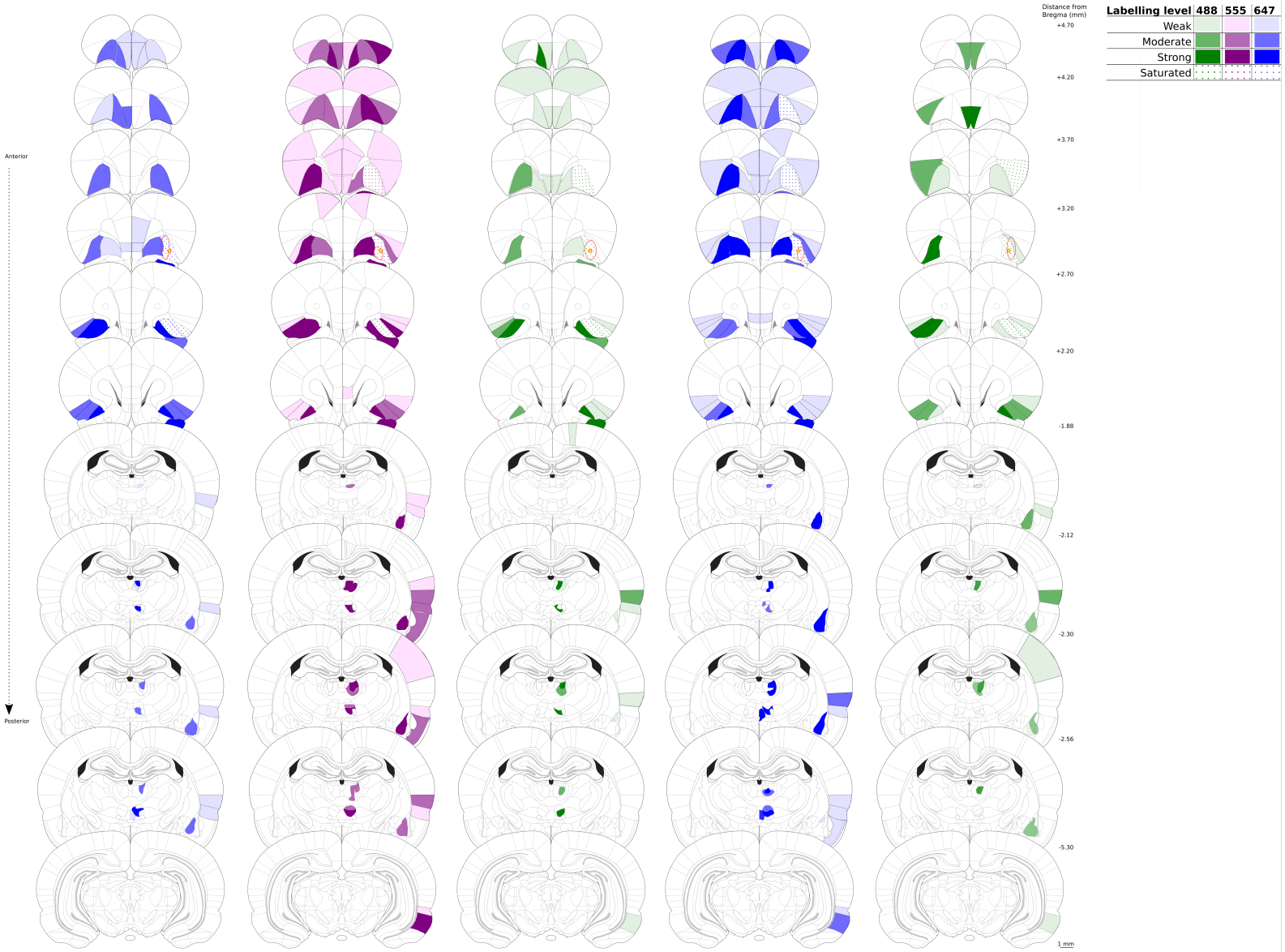

Figure S3. **Density of retrogradely-labelled cells following CTB injection into PLO.** Lighter or darker shades represent lower or higher labelling densities, respectively. Red star and oval shapes represent the intended and the observed injection sites core, respectively. Brains are sorted by the location of its observed injection site, from medial to lateral. CTB: cholera toxin subunit B; PLO: orbitofrontal cortex, posterior lateral area; 488: Alexa Fluor 488; 555: Alexa Fluor 555; 647: Alexa Fluor 647.

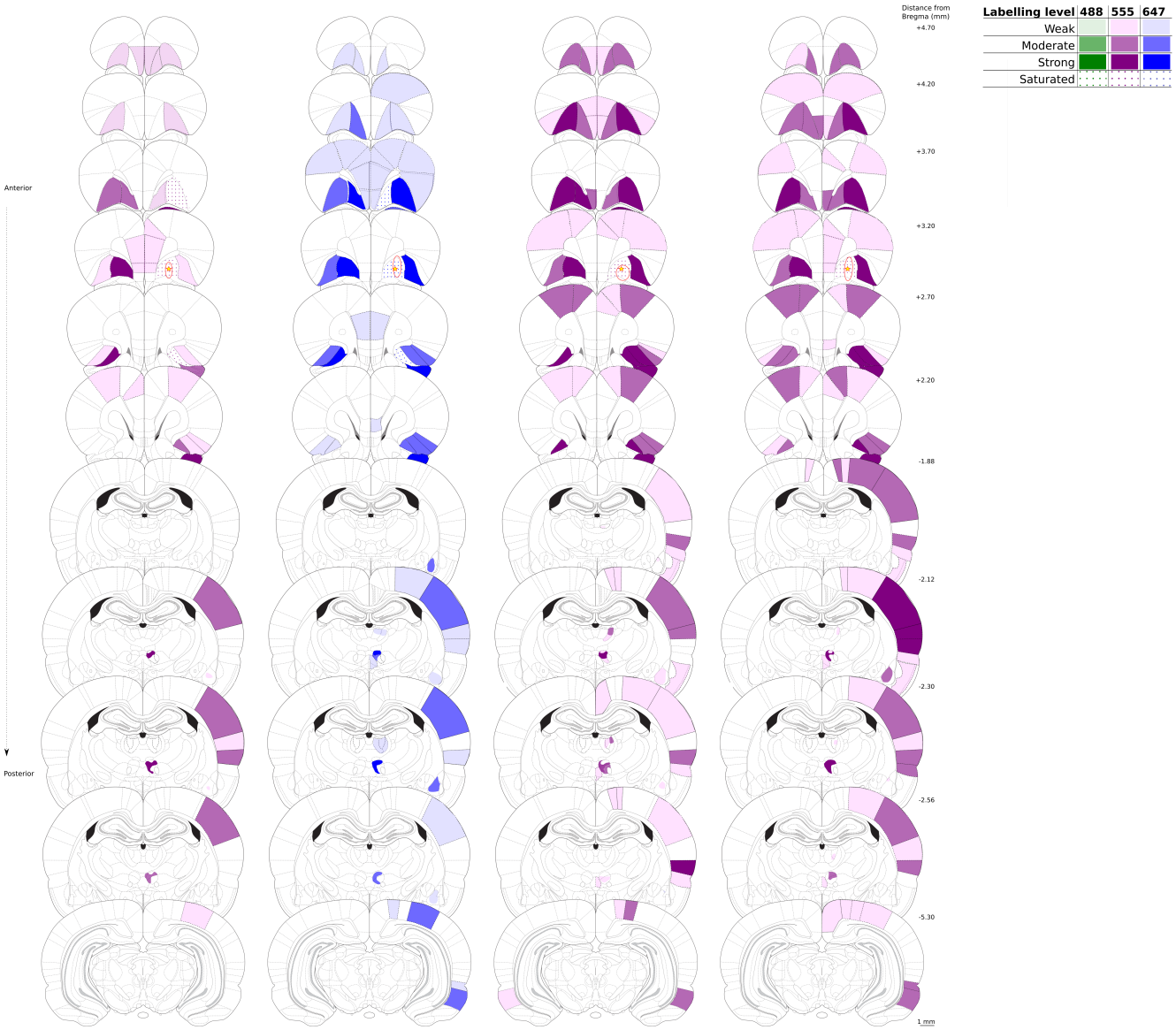

Figure S4. **Density of retrogradely-labelled cells following CTB injection into PVO.** Lighter or darker shades represent lower or higher labelling densities, respectively. Red star and oval shapes represent the intended and the observed injection sites core, respectively. Brains are sorted by the location of its observed injection site, from medial to lateral. CTB: cholera toxin subunit B; PVO: orbitofrontal cortex, posterior lateral area; 488: Alexa Fluor 488; 555: Alexa Fluor 555; 647: Alexa Fluor 647.

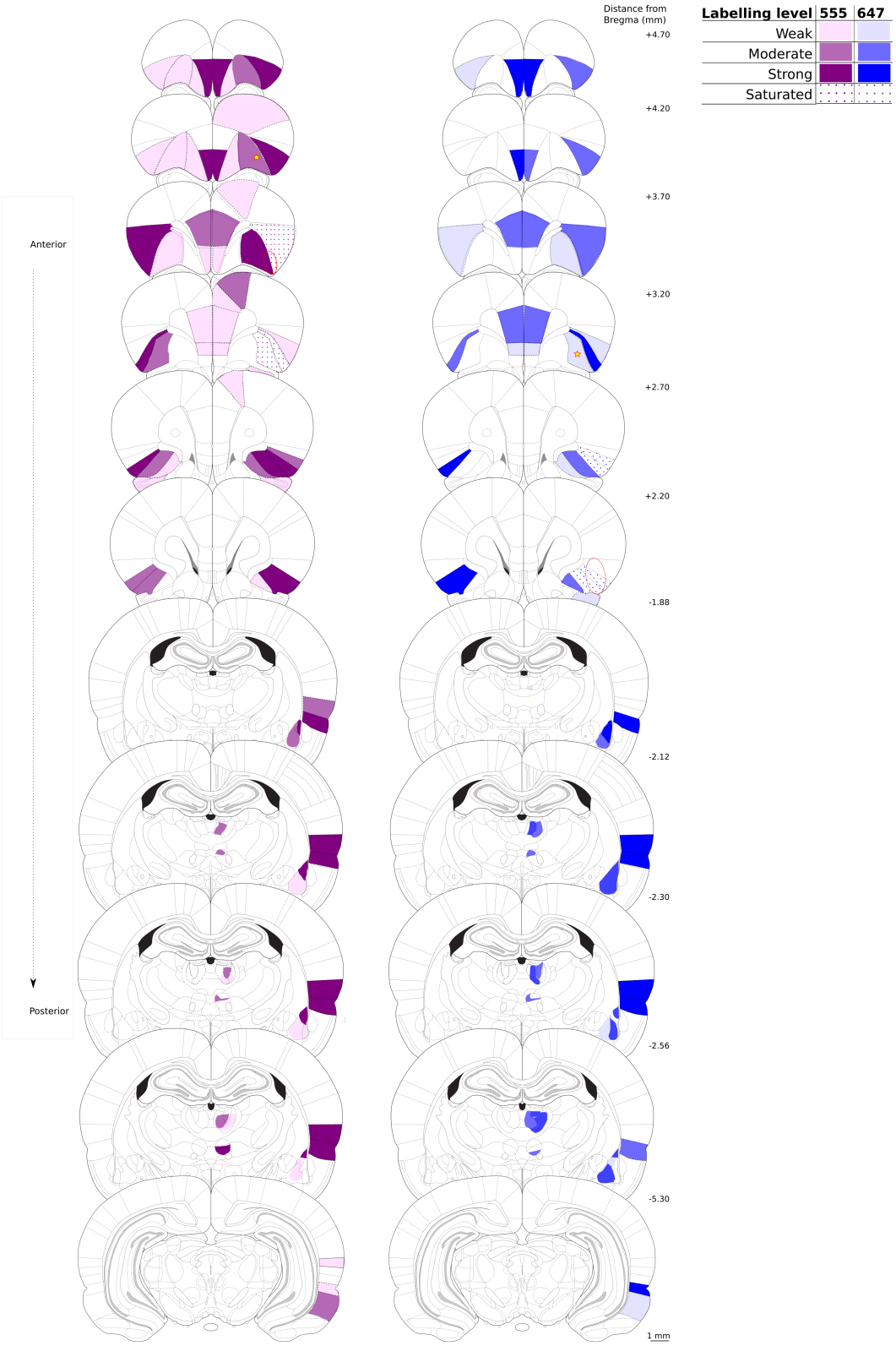

Figure S5. **Density of retrogradely-labelled cells following injection of CTB coupled to alexa-fluor 555 or 648 conjugate, into brain 23.** Lighter or darker shades represent lower or higher labelling densities, respectively. Red star and oval shapes represent the intended and the observed injection sites core, respectively. CTB: cholera toxin subunit B; 555: Alexa Fluor 555; 647: Alexa Fluor 647.